iScience

CellPress
OPEN ACCESS

Article

Adam10-dependent Notch signaling establishes dental epithelial cell boundaries required for enamel formation

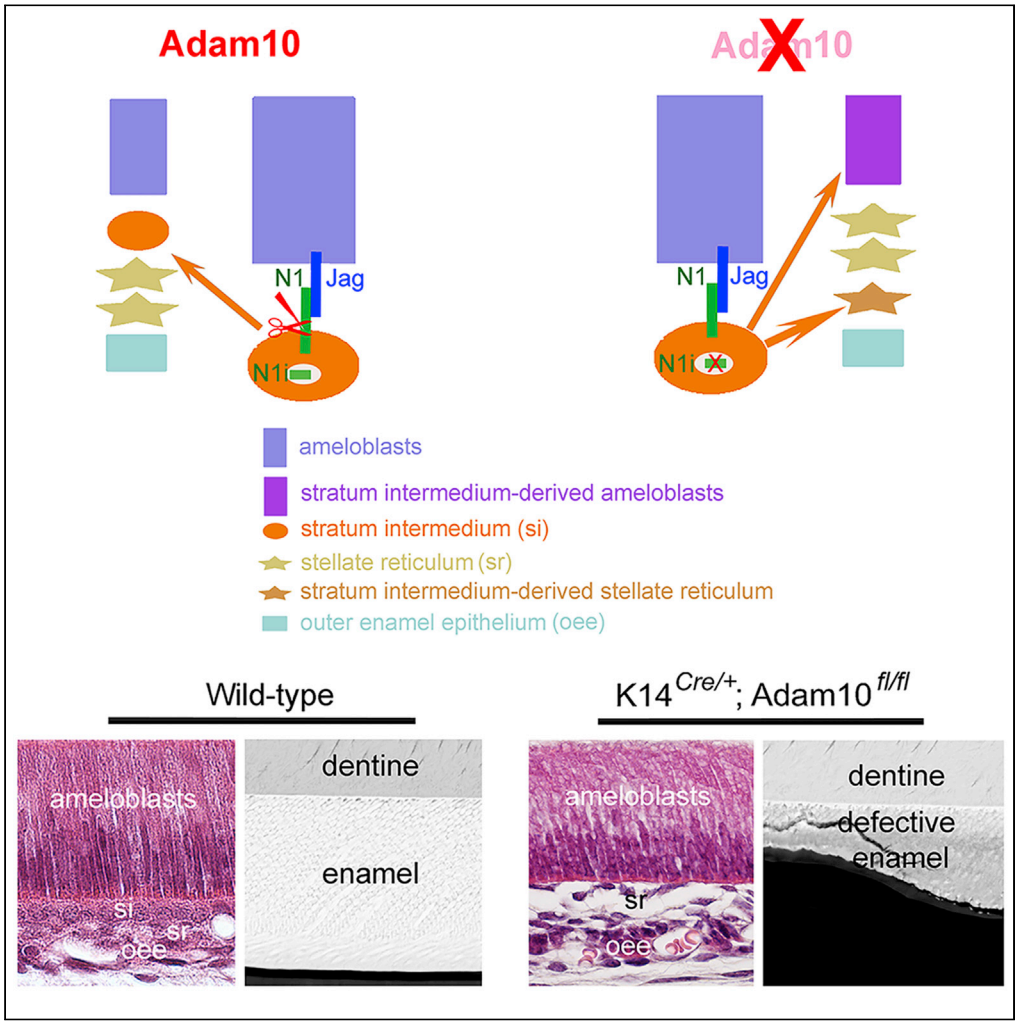

Thimios A. Mitsiadis, Lucia Jimenez-Rojo, Anamaria Balic, Silvio Weber, Paul Saftig, Pierfrancesco Pagella

thimios.mitsiadis@zzm.uzh.ch

Highlights

ADAM10 deletion in the dental epithelium causes the formation of defective enamel

ADAM10 deletion leads to loss of stratum intermedium and *Notch1* expression

ADAM10 deletion leads to stratum intermedium-to-ameloblast cell fate switch

Mitsiadis et al., iScience *25*, 105154
October 21, 2022
https://doi.org/10.1016/j.isci.2022.105154

iScience

CellPress
OPEN ACCESS

Article

Adam10-dependent Notch signaling establishes dental epithelial cell boundaries required for enamel formation

Thimios A. Mitsiadis,[1,4,*] Lucia Jimenez-Rojo,[1] Anamaria Balic,[1] Silvio Weber,[2] Paul Saftig,[3] and Pierfrancesco Pagella[1]

SUMMARY

The disintegrin and metalloproteinase Adam10 is a membrane-bound sheddase that regulates Notch signaling and ensures epidermal integrity. To address the function of Adam10 in the continuously growing incisors, we used Keratin14$^{Cre/+}$;Adam10$^{fl/fl}$ transgenic mice, in which Adam10 is conditionally deleted in the dental epithelium. Keratin14$^{Cre/+}$;Adam10$^{fl/fl}$ mice exhibited severe abnormalities, including defective enamel formation reminiscent of human enamel pathologies. Histological analyses of mutant incisors revealed absence of stratum intermedium, and severe disorganization of enamel-secreting ameloblasts. *In situ* hybridization and immunostaining analyses in the Keratin14$^{Cre/+}$;Adam10$^{fl/fl}$ incisors showed strong *Notch1* downregulation in dental epithelium and ectopic distribution of enamel-specific molecules, including ameloblastin and amelogenin. Lineage tracing studies using Notch1^{CreERT2};R26$^{mT/mG}$ mice demonstrated that loss of the stratum intermedium cells was due to their fate switch toward the ameloblast lineage. Overall, our data reveal that in the continuously growing incisors the Adam10/Notch axis controls dental epithelial cell boundaries, cell fate switch and proper enamel formation.

INTRODUCTION

The highly conserved Notch intracellular signaling pathway regulates cell fate determination, proliferation and differentiation, thereby maintaining homeostasis in a variety of tissues and organs (Andersson et al., 2011; Artavanis-Tsakonas et al., 1995, 1999; Artavanis-Tsakonas and Muskavitch, 2010; Guruharsha et al., 2012; Hori et al., 2013; Kopan, 2012). Four Notch receptors (Notch1-4) and five Notch membrane-bound ligands (Jag1, Jag2, Dll1, Dll3, and Dll4) have been identified in mammals (Fleming et al., 1997; Gray et al., 1999; Kopan and Ilagan, 2009; Nye and Kopan, 1995; Siebel and Lendahl, 2017). Upon ligand binding, the extracellular juxtamembrane domain of Notch protein is proteolytically cleaved by the membrane-anchored enzyme Adam10 (a disintegrin and metalloprotease 10) (Guruharsha et al., 2012; Hori et al., 2013; Kopan and Ilagan, 2009; Kovall et al., 2017; Weber and Saftig, 2012). This enables γ-secretase processing and release of the Notch intracellular domain, which subsequently translocates into the nucleus, where it functions as a transcriptional activator (Andersson et al., 2011; Artavanis-Tsakonas et al., 1999; Guruharsha et al., 2012; Kopan, 2012; Kovall et al., 2017). Previous *in vivo* studies have demonstrated that Adam10 is essential for the integrity of various epithelial structures through regulation of Notch-mediated signaling (Kaplan et al., 2018; Sakamoto et al., 2021; Weber et al., 2011; Weber and Saftig, 2012). Adam10 also sheds E-cadherin and participates in its asymmetric distribution, which affects cell migration and compartmentalization in the intestinal (Solanas et al., 2011) and incisor's epithelium (Li et al., 2012). Cell-autonomous Adam10 activity in intestine is required for Notch signaling-dependent regulation of stem cells and cell lineage specification (Tsai et al., 2014). In addition, Adam10 plays a crucial role in both the immune system (Lambrecht et al., 2018) and longitudinal bone growth (Mizuno et al., 2020). However, the function of Adam10 in dental tissues is poorly understood.

Rodent teeth (i.e., molars and the continuously growing incisors) represent powerful biological models for studying the molecular mechanisms involved in cell fate specification and differentiation of various cell lineages (Mitsiadis and Graf, 2009). Reciprocal inductive interactions between the epithelial cells and the underlying neural crest-derived mesenchyme give rise to diverse cell types that progressively form the

[1]Orofacial Development and Regeneration, Institute of Oral Biology, Centre for Dental Medicine, University of Zurich, Plattenstrasse 11, 8032 Zurich, Switzerland

[2]Miltenyi Biotec B.V. & Co. KG, 51429 Bergisch Gladbach, Germany

[3]Biochemical Institute, Christian-Albrechts-Universität Kiel, 24118 Kiel, Germany

[4]Lead contact

*Correspondence: thimios.mitsiadis@zzm.uzh.ch

https://doi.org/10.1016/j.isci.2022.105154

complex dental structures (Balic and Thesleff, 2015; Cobourne and Mitsiadis, 2006; Pagella et al., 2020; Yu and Klein, 2020). Specifically, the dental epithelium is composed of four distinct cell layers, including the outer dental epithelium, stratum intermedium, stellate reticulum and inner dental epithelium/ameloblasts (Mitsiadis and Graf, 2009). Ameloblast layer is responsible for the formation of enamel, which is the most mineralized tissue of the body (Bartlett, 2013; Smith and Nanci, 1995). Our previous studies have shown that during odontogenesis the expression patterns of Notch receptors and ligands are restricted and complementary in dental epithelium (Mitsiadis et al., 1995, 1997, 1998, 2005, 2010). *Notch1* expression is confined to stratum intermedium (Mitsiadis et al., 1995), whereas *Dll1* and *Jag2* are both expressed in the adjacent inner enamel epithelium/ameloblasts (Mitsiadis et al., 1998, 2010), thus reflecting the subdivision of the dental epithelium into ameloblast and non-ameloblast layers. These results suggest that Notch signaling controls amelogenesis and regulates dental epithelial cell fate specification and differentiation events. Conversely, it was recently shown that *Notch1*-expressing cells in the stratum intermedium represent a reservoir of dental epithelial progenitors that are activated upon tooth injury and contribute to the regeneration of the ameloblast layer (Sharir et al., 2019). *Adam10* expression in ameloblasts was recently reported, and *in vitro* results suggested a role for this molecule in the regulation of enamel secretion (Ikeda et al., 2019).

To further address the function of Adam10 and its relevance in Notch-mediated signaling during amelogenesis, we used transgenic mouse models in which *Adam10* is conditionally deleted in the dental epithelium (Weber et al., 2011), as well as GI254023X, an Adam10 inhibitor. We found that the loss of Adam10 activity in the Keratin14$^{Cre/+}$;Adam10$^{fl/fl}$ mice affects tooth enamel formation. This phenotype is associated with the loss of the stratum intermedium cells and the concomitant downregulation of *Notch1* expression. Using Notch1^{CreERT2};R26$^{mT/mG}$ mice (Fre et al., 2011), we demonstrated that epithelial Adam10 deletion induces a cell fate switch of stratum intermedium cells toward ameloblasts. Conclusively, our data show that the Adam10/Notch1 signaling axis is crucial for establishing dental epithelial cell fates and essential for accurate enamel formation.

RESULTS

Deletion of Adam10 leads to defective enamel formation

We first analyzed *Adam10* expression using *in situ* hybridization in postnatal mouse incisors (P1-P2). *Adam10* mRNA was mainly expressed in stratum intermedium, inner enamel epithelial cells, including preameloblasts and ameloblasts (Figures S1A and S1B). At the protein level, Adam10 was distributed in stratum intermedium cells, preameloblasts and ameloblasts in P1-P6 incisors (Figures S1C–S1F). As the ameloblast differentiation advances, Adam10 staining intensified in ameloblasts, whereas it decreased in the stratum intermedium (Figures S1D–S1F). Surprisingly, strong Adam10 labeling was also observed in the enamel (Figures S1E, S1G, S1H), which suggests that either fragments of Adam10 protein are trapped within newly forming enamel or non-specific immunostaining. To elucidate these unexpected findings, mass spectrometry analyses should be realized in the future.

Next, we studied the role of Adam10 in amelogenesis by assessing the enamel of incisors from K14$^{Cre/+}$;Adam10$^{fl/fl}$ mice, in which Adam10 is conditionally knocked out from dental epithelium. The enamel of wild-type mouse incisors is characterized by a yellowish-reddish pigmentation due to iron deposits (Figures 1A and 1B), which increase the hardness of enamel (Gordon et al., 2015). In contrast, mutant incisors displayed a translucent/white enamel (Figures 1A′, 1B′) that indicates a crucial role for Adam10 in the enamel synthesis and composition. We therefore studied in detail the enamel defects observed in the K14$^{Cre/+}$;Adam10$^{fl/fl}$ incisors by micro-CT (μCT), scanning electron microscopy (SEM) and histological examination.

Enamel situated at the labial side of the incisors is visualized in SEM and μCT as a bright white layer that indicates the elevated mineral content of this tissue. In wild-type mice, the enamel layer was clearly defined in both longitudinal and frontal orientations of the incisors (Figure 1C). In contrast, the enamel was not visible in the mutant incisors, although a very thin white layer was observed sporadically at their anterior part (Figure 1C′). Further SEM analysis indicated mineral and structural disorganization of the K14$^{Cre/+}$;Adam10$^{fl/fl}$ enamel. Indeed, the enamel of mutant incisors was thinner, severely hypocalcified and disorganized (notably in the orientation, arrangement and thickness of the enamel rods) when compared to the wild-type enamel (Figures 1D, 1D′). The degree of hard tissue mineralization can be estimated upon staining with Toluidine Blue (TB), which is retained by the organic matrix of the tissue. The

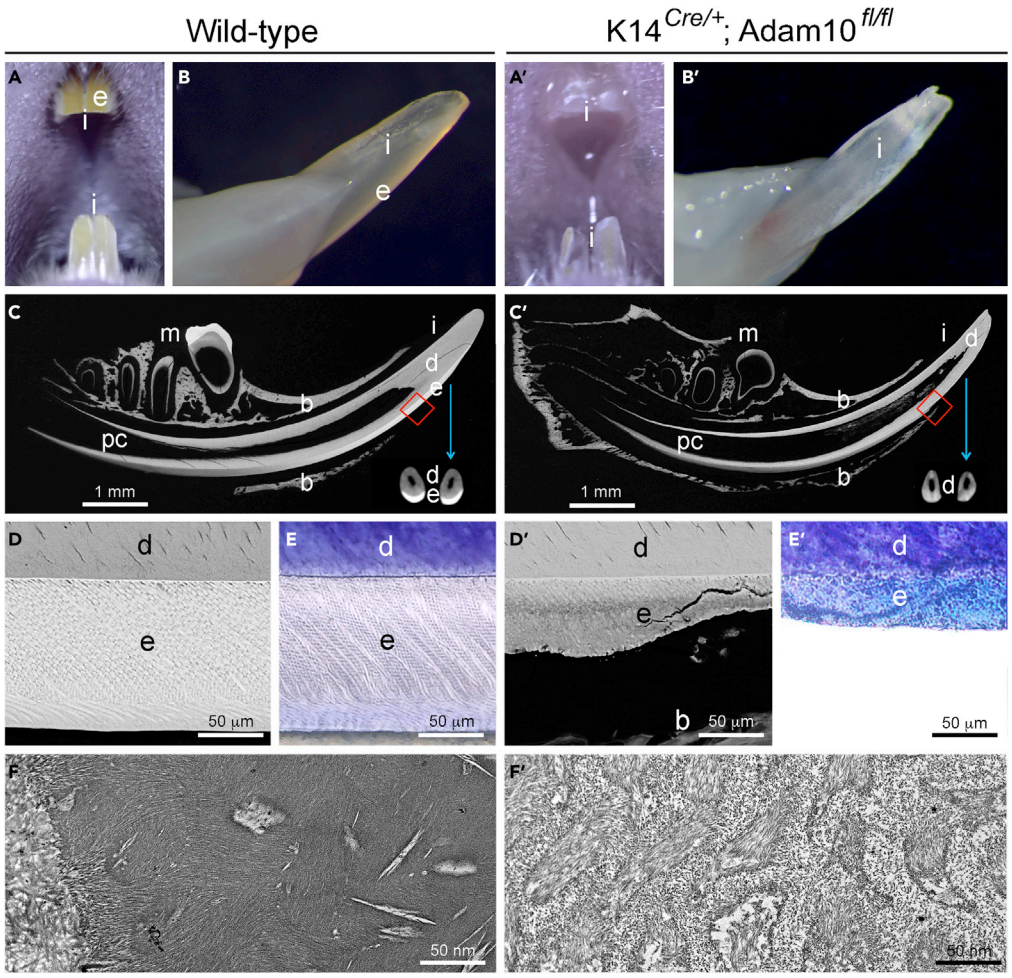

Figure 1. *Adam10* deletion in the dental epithelium causes enamel defects

(A-B′) Macroscopic views of wild-type (A, B) and K14$^{Cre/+}$;Adam10$^{fl/fl}$ (A′, B′) incisors. Mutant incisors appear white/transparent (compare A with A′, and B with B′).

(C, C′) Scanning Electron Microscopy (SEM) images of lower jaws from wild-type (C) and mutant (C′) mice. Images in the lower right corner are sections from wild-type and mutant jaws processed by Microcomputed Tomography (μCT).

(D, D′) High magnification SEM images of red boxed areas on the labial side of the incisors in (C) and (C′), showing normal enamel in wild-type incisors (D) and the hypoplastic and hypomineralized enamel in K14$^{Cre/+}$;Adam10$^{fl/fl}$ incisors (D′).

(E, E′) Toluidine blue staining in ground sections showing the well-structured white (absence of organic matrix) enamel in wild-type incisors (E) and deficient blue stained (high levels of organic matrix) enamel in K14$^{Cre/+}$; Adam10$^{fl/fl}$ incisors (E′).

(F, F′) High magnification transmission electron microscopy (TEM) images showing enamel crystals and intercrystallite spaces in wild-type (F) and K14$^{Cre/+}$;Adam10$^{fl/fl}$ (F′) incisors. Notice the existence of large intercrystallite spaces in the enamel of mutant incisors (F′). Abbreviations: b, bone; d, dentine; e, enamel; i, incisor; m, molar; pc, pulp chamber.

enamel of wild-type incisors, due to its high mineral content, did not retain the dye and exhibited a white color (Figure 1E). In contrast, the enamel layer of the mutant incisors acquired a blue appearance after TB staining (Figure 1E′), indicating a less mineralized enamel rich in organic elements. Transmission electron microscopy (TEM) analyses revealed defective enamel maturation in mutant incisors. Compared to the wild-type enamel, broader intercrystallite spaces appeared in the mutant enamel, due to the incapacity of enamel crystals to increase in width and thickness (Figures 1F, 1F′).

Disorganized ameloblasts and ectopic enamel matrix deposition in Adam10 mutant incisors

To investigate the cellular mechanisms that underlie the enamel phenotype in the K14$^{Cre/+}$;Adam10$^{fl/fl}$ incisors, we analyzed histological sections of wild-type and K14$^{Cre/+}$;Adam10$^{fl/fl}$ incisors (Figures 2A-2B′ and S2). Amelogenesis is a complex process that requires the differentiation of inner enamel epithelium cells

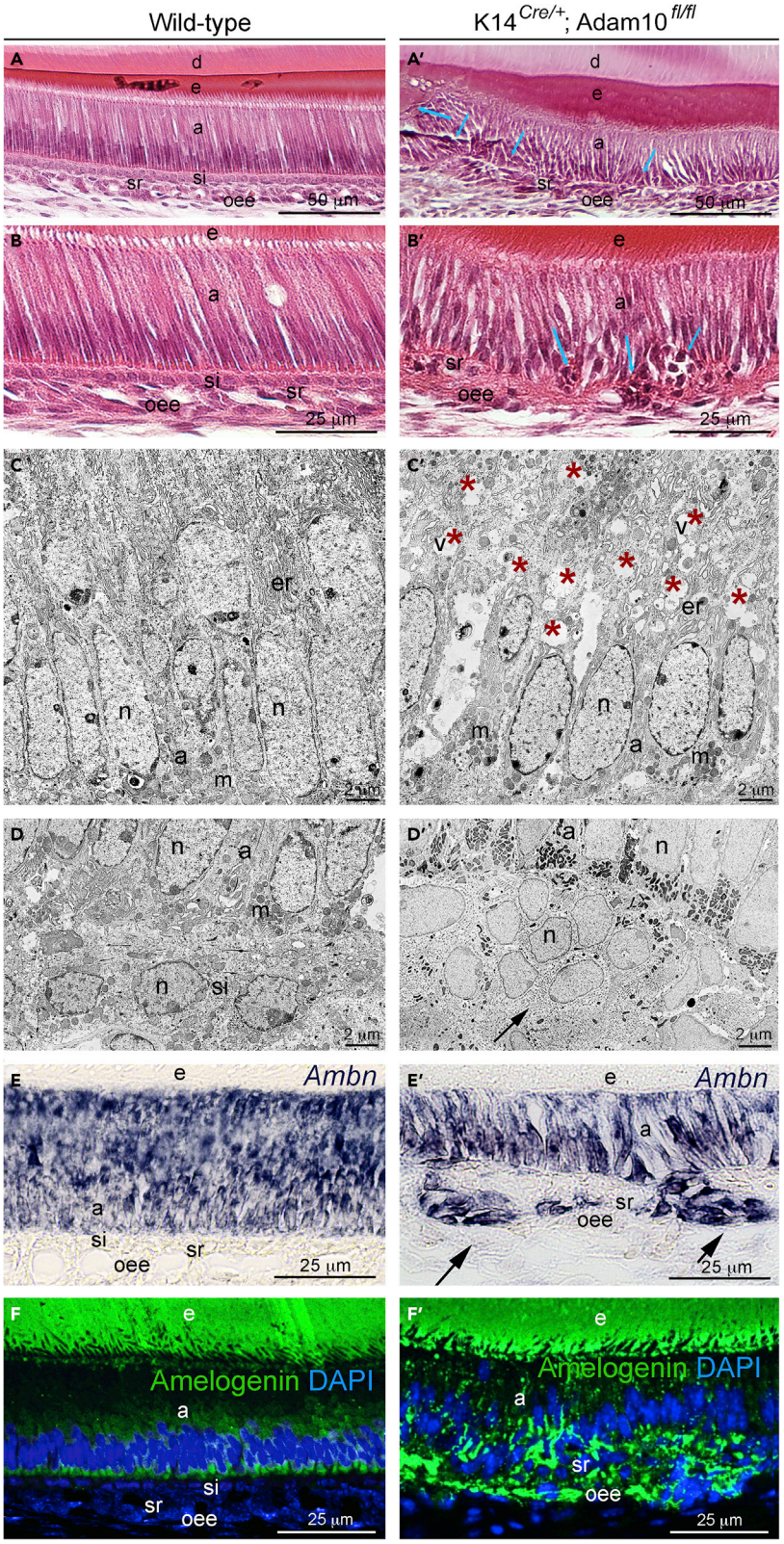
Wild-type
K14Cre/+; Adam10fl/fl
A
d
e
a
sr
si
oee
50 μm
A′
d
e
a
sr
oee
50 μm
B
e
a
si
oee
sr
25 μm
B′
e
a
sr
oee
25 μm
C
er
n
n
a
m
2 μm
C′
v
v
er
n
m
a
m
2 μm
D
n
a
m
n
si
2 μm
D′
a
n
n
2 μm
E
e
Ambn
a
si
oee
sr
25 μm
E′
e
Ambn
a
sr
oee
25 μm
F
e
Amelogenin DAPI
a
si
sr
oee
25 μm
F′
e
Amelogenin DAPI
a
sr
oee
25 μm

Figure 2. *Adam10* deletion induces disorganization of the ameloblast layer, loss of ameloblasts polarity and ectopic enamel secretion

(A-B′) Hematoxylin and eosin (H&E) staining of wild-type (A, B) and K14$^{Cre/+}$;Adam10$^{fl/fl}$ (A′, B′) incisors. Blue arrows indicate areas of ectopically formed cell clusters (A′, B′). Higher magnification H&E images showing ameloblasts orientation in wild-type (B) and K14$^{Cre/+}$;Adam10$^{fl/fl}$ (B′) incisors.

(C, C′) TEM analysis of ameloblasts from wild-type (C) and K14$^{Cre/+}$;Adam10$^{fl/fl}$ (C′) incisors demonstrating the increased number of vacuoles (red asterisks) and empty spaces in the ameloblasts of K14$^{Cre/+}$;Adam10$^{fl/fl}$ incisors (C′).

(D, D′) TEM images of structures adjacent to ameloblast layer from C and C′ of wild-type (D) and K14$^{Cre/+}$;Adam10$^{fl/fl}$ (D′) incisors, demonstrating intact stratum intermedium in wild-type incisors (D), and the presence of cell clusters (black arrow) in K14$^{Cre/+}$;Adam10$^{fl/fl}$ incisors (D′).

(E, E′) *In situ* hybridization showing expression of *Ambn* (violet color) in the wild-type (E) and K14$^{Cre/+}$;Adam10$^{fl/fl}$ (E′) incisors. In K14$^{Cre/+}$;Adam10$^{fl/fl}$ incisors, *Ambn* is expressed by ameloblasts and clusters of dental epithelial cells (black arrows in E′).

(F, F′) Immunofluorescent staining showing distribution of the Amelogenin protein (green color) =in wild-type (F) and K14$^{Cre/+}$;Adam10$^{fl/fl}$ (F′) incisors. Cell nuclei are identified by DAPI (blue color). Abbreviation: a, ameloblasts; d, dentine; e, enamel; er, endoplasmic reticulum; m, mitochondria; n, nucleus; oee, outer enamel epithelium; si, stratum intermedium; sr, stellate reticulum; v, vacuoles.

into preameloblasts/ameloblasts and the orchestration of fine-tuned events involved in the secretion of enamel specific matrices and deposition of minerals in order to generate the unique and well-organized enamel tissue (Gordon and Joester, 2015). Histological sections stained with hematoxylin and eosin (H&E) showed that the ameloblast layer is completely disordered in the K14$^{Cre/+}$;Adam10$^{fl/fl}$ incisors when compared to the well-organized ameloblast layer of wild-type incisors (compare Figures 2A, 2B to 2A′, 2B′ and S2A, S2B to S2A′, S2B′). In wild-type incisors, functional ameloblasts were elongated and oriented perpendicularly to the deposited enamel (Figures2A, 2B, S2B and S3A). By contrast, in K14$^{Cre/+}$;Adam10$^{fl/fl}$ incisors the ameloblast layer was highly disoriented and depolarized (Figures 2A′, 2B′, S2B′ and S3A). This disorder in the ameloblast layer was frequently associated with the formation of cell clusters (blue arrows in Figures 2A′, 2B′). TEM examination showed an increased number of vacuoles and empty spaces in the ameloblasts of the K14$^{Cre/+}$;Adam10$^{fl/fl}$ incisors (red asterisks in Figure 2C′), when compared to the wild-type incisors (compare Figures 2C–2C′). TEM also confirmed the formation of cell clusters (black arrow in Figure 2D′) localized next to the basal side of ameloblasts, where stratum intermedium is positioned in the wild-type incisors (compare Figures 2D–2D′).

To further characterize the effects of Adam10 deletion in amelogenesis we performed comparative expression analyses of molecules fundamental for enamel formation (i.e., Ameloblastin and Amelogenin) in wild-type and K14$^{Cre/+}$;Adam10$^{fl/fl}$ incisors. *In situ* hybridization showed the expression of the enamel-specific gene *Ambn* (coding for the Ameloblastin protein) in ameloblasts of the wild-type incisors (Figure 2E), whereas in the K14$^{Cre/+}$;Adam10$^{fl/fl}$ incisors *Ambn* was expressed in both ameloblasts and cell clusters that are formed outside of the ameloblast layer (Figure 2E′). Similarly, immunofluorescent staining with Amelogenin in wild-type incisors clearly demonstrated the presence of this enamel specific protein in both ameloblasts and enamel (Figure 2F), whereas in the K14$^{Cre/+}$;Adam10$^{fl/fl}$ incisors the staining was detected in all dental epithelial cell populations and the enamel (Figure 2F′).

Loss of the stratum intermedium layer in incisors of Adam10 mutant mice

Next, we analyzed the effects of *Adam10* deletion on the other cell layers that compose the dental epithelium using histological sections of incisors stained with either H&E or TB. The most striking observation was the absence of the stratum intermedium layer in the K14$^{Cre/+}$;Adam10$^{fl/fl}$ incisors (Figures S2A′, S2B′ and S3A′, S3B′). In wild-type incisors, stratum intermedium is composed of cuboidal-shaped cells (Figures S2A, S2B and S3A, S3B). Instead, in K14$^{Cre/+}$;Adam10$^{fl/fl}$ incisors, a layer of flat, loose cells, which closely resemble the stellate reticulum cells, was occupying the space normally allocated to stratum intermedium (compare Figures 3A, 3B, to 3A′, 3B′). TEM analyses confirmed the absence of stratum intermedium cells and the existence of a loose epithelial tissue in K14$^{Cre/+}$;Adam10$^{fl/fl}$ incisors (compare Figures 3C–3C′).

Because *Notch1* is specifically expressed by stratum intermedium cells in rodent teeth (Mitsiadis et al., 1995, 1998), and Adam10 is a key modulator of Notch signaling activation, we wished to know if *Notch1* expression persists in K14$^{Cre/+}$;Adam10$^{fl/fl}$ incisors. Therefore, we analyzed and compared *Notch1* expression in wild-type and K14$^{Cre/+}$;Adam10$^{fl/fl}$ incisors using *in situ* hybridization. In the epithelium of wild-type

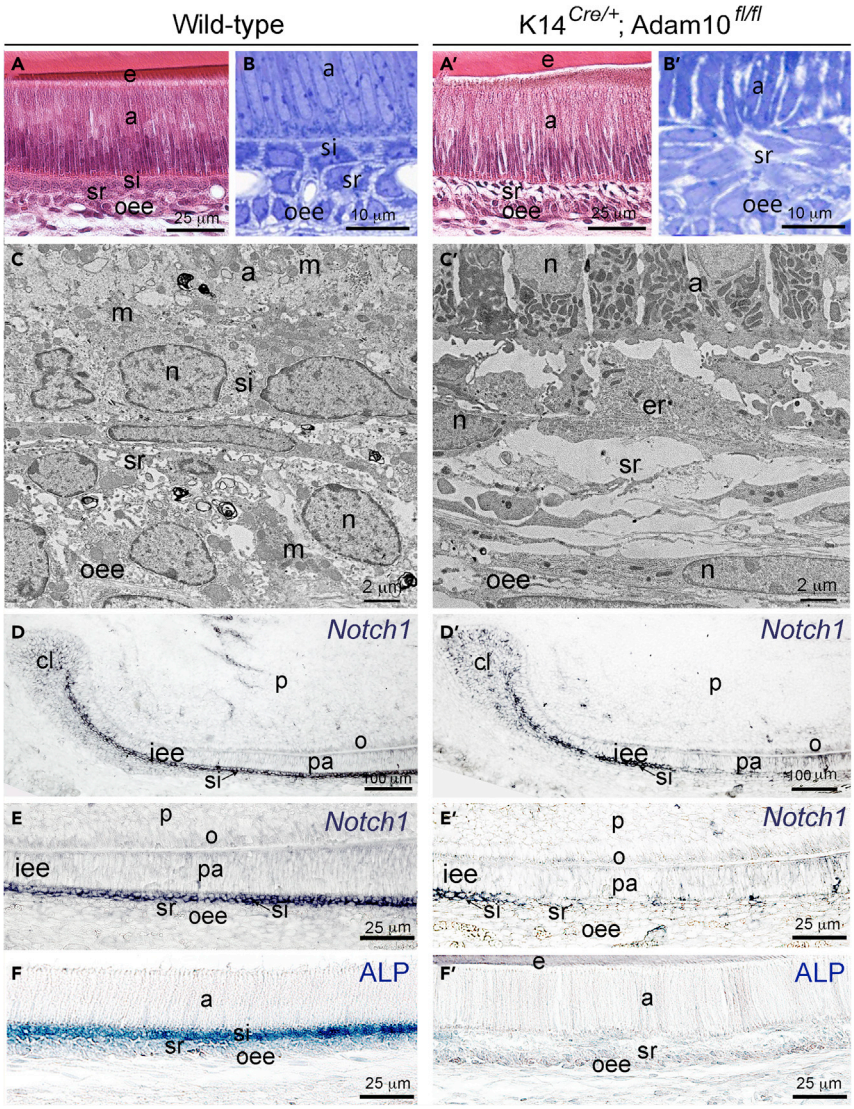

Figure 3. *Adam10* deletion induces loss of the stratum intermedium, downregulation of the *Notch1* expression and loss of the Alkaline Phosphatase (ALP) activity

(A, A′) H&E staining of wild-type (A) and K14$^{Cre/+}$;Adam10$^{fl/fl}$ (A′) incisors.

(B, B′) High magnification images of Toluidine blue staining in wild-type (B) and K14$^{Cre/+}$;Adam10$^{fl/fl}$ (B′) incisors.

(C, C′) TEM images of the interface between ameloblasts and stratum intermedium in wild-type incisors (C) and the interface between ameloblasts and stellate reticulum cells in K14$^{Cre/+}$;Adam10$^{fl/fl}$ incisors (C′).

(D-D′) *In situ* hybridization showing *Notch1* expression in wild-type (D) and K14$^{Cre/+}$;Adam10$^{fl/fl}$ (D′) incisors. Notice that in K14$^{Cre/+}$;Adam10$^{fl/fl}$ incisors, *Notch1* expression is downregulated outside of the cervical loop area, soon after the onset of dental epithelial cell differentiation.

(E, E′) Higher magnifications of dental epithelial cells layers from D and D′, respectively, demonstrating downregulated *Notch1* expression following differentiation of inner enamel epithelium cells into preameloblasts.

(F, F′) ALP staining in wild-type (F) and K14$^{Cre/+}$;Adam10$^{fl/fl}$ (F′) incisors, from the region of differentiating ameloblasts.

Abbreviations: a, ameloblasts; b, bone; cl, cervical loop; d, dentine; e, enamel; er, endoplasmic reticulum; i, incisor; iee, inner enamel epithelium; m, mitochondria; n, nucleus; o, odontoblasts; oee, outer enamel epithelium; p, dental pulp; pa, preameloblasts; si, stratum intermedium; sr, stellate reticulum.

incisors, *Notch1* was intensively and exclusively expressed by cells of the stratum intermedium (Figures 3D and 3E). In contrast, *Notch1* expression was significantly downregulated in the remaining stratum intermedium cells at the posterior part of K14$^{Cre/+}$;Adam10$^{fl/fl}$ incisors whereas the expression completely disappeared in the median and anterior parts of the K14$^{Cre/+}$;Adam10$^{fl/fl}$ incisor's epithelium (Figures 3D′,

3E′). We additionally used Alkaline Phosphate (ALP), which is a well-established marker of stratum intermedium cells (Larsson, 1976), to confirm their absence in K14$^{Cre/+}$;Adam10$^{fl/fl}$ incisors. Although ALP activity strongly labeled the stratum intermedium cell layer in wild-type incisors (Figure 3F), it was missing in the epithelium of K14$^{Cre/+}$;Adam10$^{fl/fl}$ incisors (Figure 3F).

In situ hybridization revealed that *Adam10* deletion also affected *Notch2* expression in the epithelium of K14$^{Cre/+}$;Adam10$^{fl/fl}$ incisors. In wild-type incisors, strong *Notch2* hybridization signal is exclusively detected in stellate reticulum (Figures S4A, S4B). In contrast, diffused *Notch2* expression is observed in all epithelial cell layers of the K14$^{Cre/+}$;Adam10$^{fl/fl}$ incisors, with hotspots of reactivity in stratum intermedium and outer enamel epithelium cells (Figures S4A′, S4B′).

In addition, using a specific anti-Notch1 antibody that exclusively detects the extracellular domain of this molecule (Mitsiadis et al., 1995), we analyzed its distribution in the wild-type and K14$^{Cre/+}$;Adam10$^{fl/fl}$ incisors. In wild-type incisors, immunoreactivity for the Notch1 extracellular domain is localized exclusively at the basal end of ameloblasts (Figure S4C), which indicates the internalization of this fragment released upon Notch1 cleavage (Hori et al., 2013). In contrast, Notch1 staining was absent in the epithelium of K14$^{Cre/+}$;Adam10$^{fl/fl}$ incisors (Figure S4C′). Similarly, strong Notch2 staining was detected in stellate reticulum and outer enamel epithelium cells of the wild-type incisors (Figure S4D) whereas a weaker and diffused labeling was observed in these cell layers of K14$^{Cre/+}$;Adam10$^{fl/fl}$ incisors (Figure S4D′).

Loss of *Adam10* affects cell proliferation but not apoptotic events in dental epithelium

The disappearance of stratum intermedium cells in the K14$^{Cre/+}$;Adam10$^{fl/fl}$ incisors could be linked to apoptotic events. To test this hypothesis, we performed TUNEL assay that allows the detection of abnormal cell death in the dental epithelium of K14$^{Cre/+}$;Adam10$^{fl/fl}$ incisors, and most specifically in the area attributed to the stratum intermedium layer in wild-type incisors (Figures 4A-4B′). However, we did not observe any apoptotic activity in the dental epithelium of either wild-type (Figures 4A and 4B) or K14$^{Cre/+}$;Adam10$^{fl/fl}$ incisors (Figures 4A′, 4B′). TUNEL staining was observed in sections of other tissues of wild-type and K14$^{Cre/+}$;Adam10$^{fl/fl}$ mice (e.g. skin) that were used as positive controls (Figures S5A, S5B).

Because Notch signaling is involved in proliferative events (Artavanis-Tsakonas et al., 1995; Ho and Artavanis-Tsakonas, 2016), we examined if *Notch* deregulation affected dental epithelial cell proliferation in the K14$^{Cre/+}$;Adam10$^{fl/fl}$ incisors using Phospho-Histone 3 (pH3) immunofluorescent staining. In the wild-type incisors, pH3 labeling was detected in few cells of the stratum intermedium and in preameloblasts (Figures 4C and 4D) whereas in K14$^{Cre/+}$;Adam10$^{fl/fl}$ incisors, abundant pH3 staining was restricted to preameloblasts (Figures 4C′, 4D′). Quantification of pH3 staining showed a statistically significant increase of the mitotic events in K14$^{Cre/+}$;Adam10$^{fl/fl}$ incisor's epithelium (insert in Figure 4D′). This increased number of cell divisions within the preameloblast layer in the K14$^{Cre/+}$;Adam10$^{fl/fl}$ incisors could contribute to the expansion of the number of ameloblasts and the subsequent folding of the dental epithelium to compensate for the increased cell number. To test this hypothesis, whole mount imaging was performed in K14$^{Cre/+}$;R26$^{mT/mG}$ (control; Figure 4E) and K14$^{Cre/+}$;Adam10$^{fl/fl}$;R26$^{mT/mG}$ (mutant; Figure 4E′) incisors. The 3D imaging clearly demonstrated that the dental epithelium (green color) of K14$^{Cre/+}$;Adam10$^{fl/fl}$;R26$^{mT/mG}$ incisors acquired a jagged configuration upon *Adam10* deletion (arrows in Figure 4E′).

Alterations in dental epithelium in incisors of Amelx$^{Cre/+}$;Adam10$^{fl/fl}$ and K14$^{Cre/+}$;Notch1$^{fl/fl}$ mutant mice

To study whether the tooth phenotype is due to the loss of *Adam10* function specifically in ameloblasts, we exploited Amelx$^{Cre/+}$;Adam10$^{fl/fl}$ mice, in which *Adam10* is deleted exclusively in ameloblasts (Figures S6A, S6B). μCT analysis showed normal enamel formation in Amelx$^{Cre/+}$;Adam10$^{fl/fl}$ incisors (Figure S6C). Similarly, histological sections stained with H&E showed that the dental epithelium of Amelx$^{Cre/+}$;Adam10$^{fl/fl}$ incisors did not present any alterations, neither in ameloblasts nor in stratum intermedium cells (Figures S6D, S6E). These results indicate that enamel defects observed in K14$^{Cre/+}$;Adam10$^{fl/fl}$ incisors are not due to the loss of *Adam10* function in ameloblasts, but rather to the loss of *Adam10* in progenitors and/or early precursors of preameloblast and stratum intermedium cell lineages.

We also studied whether epithelial *Notch1* deletion is able to recapitulate the tooth phenotype observed in K14$^{Cre/+}$;Adam10$^{fl/fl}$ mice. Histological examination of K14$^{Cre/+}$;Notch1$^{fl/fl}$ incisors (Figures S7A-S7C) showed that the ameloblast layer did not present any significant alterations compared to the wild-type

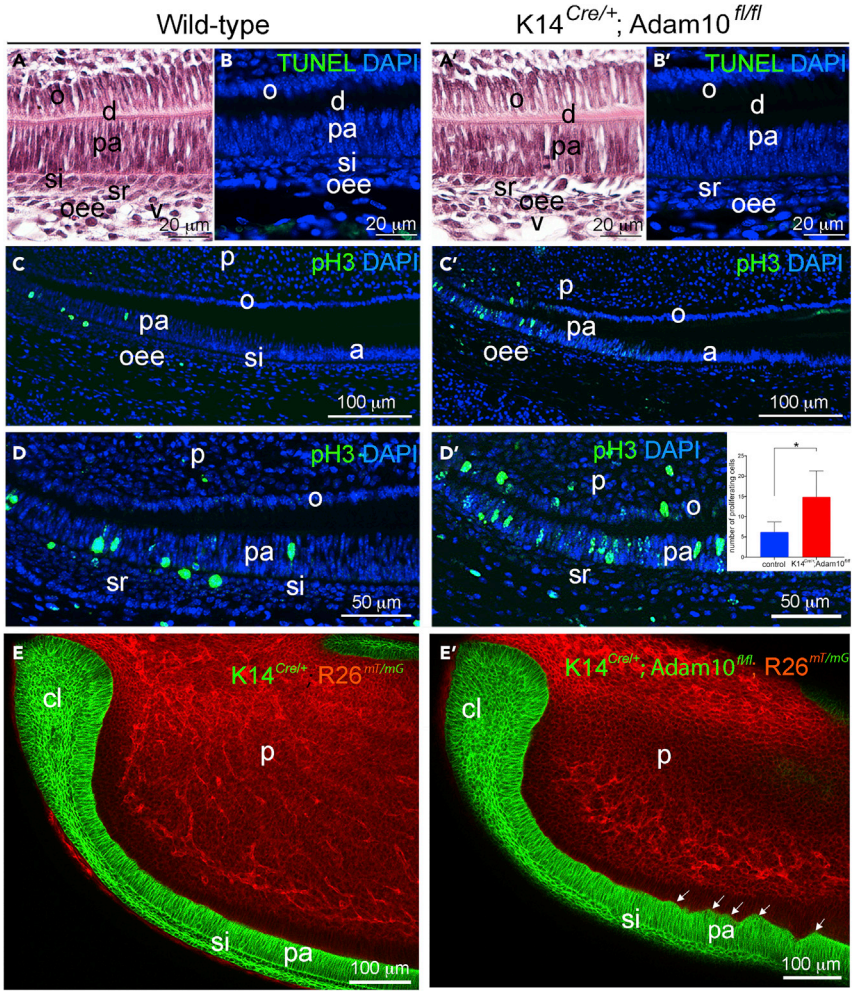

Figure 4. Adam10 deletion affects cell proliferation, but not apoptotic events

(A-B′) H&E (A, A′) and TUNEL (B, B′) staining in wild-type (A, B) and K14$^{Cre/+}$;Adam10$^{fl/fl}$ (A′, B′) incisors showing absence of cell death (green cells) in K14$^{Cre/+}$;Adam10$^{fl/fl}$ incisors (B′). DAPI staining (blue color) identifies the cell nuclei.

(C-D′) Low (C, C′) and high (D, D′) magnification images of the immunofluorescent staining against Phosphorylated Histone 3 (pH3; green color) indicates higher cell proliferation activity in the preameloblast region of K14$^{Cre/+}$;Adam10$^{fl/fl}$ incisors (C′, D′), compared to wild-type (C, D). Cell nuclei are identified by DAPI (blue color). Inserted box in (D′) shows the quantification of the number of pH3-positive cells in the preameloblast layer of the wild-type (blue color) and K14$^{Cre/+}$;Adam10$^{fl/fl}$ (red color) incisors. Asterisk (*) indicates the p value = 0.0176.

(E, E′) Whole mount imaging showing the dental epithelium in green (mGFP) in K14$^{Cre/+}$;R26$^{mT/mG}$ (E; control) and K14$^{Cre/+}$;Adam10$^{fl/fl}$;R26$^{mT/mG}$ (E′, mutant) incisors. White arrows in (E′) indicate uneven dental epithelium upon *Adam10* deletion. mTomato in red color labels the dental pulp mesenchyme. Abbreviations: a, ameloblasts; cl, cervical loop; d, dentine; e, enamel; o, odontoblasts; oee, outer enamel epithelium; p, dental pulp; pa, preameloblasts; si, stratum intermedium; sr, stellate reticulum.

incisors (Figure S7D), as previously described (Jheon et al., 2016). However, the stratum intermedium in the K14$^{Cre/+}$;Notch1$^{fl/fl}$ incisors was discontinuous, presenting both areas of ectopically formed cell clusters and territories of detachment from the ameloblast layer (arrows in Figures S7A-S7C). These results indicate a compensatory mechanism between the various Notch proteins, and thus explain the lack of severe phenotypic changes in K14$^{Cre/+}$;Notch1$^{fl/fl}$ incisors.

Treatment with an Adam10 selective inhibitor recapitulates the tooth phenotype of Adam10 mutant mice

GI254023X is a well-established Adam10 inhibitor (Hoettecke et al., 2010), and therefore we wanted to investigate if its application to wild-type incisors will recapitulate the phenotype observed in the

$K14^{Cre/+}$;$Adam10^{fl/fl}$ mutants. For this purpose, explants of isolated embryonic (E13.5) wild-type mouse incisors were cultured for 7 days *in vitro* in the presence of either DMSO (control) or the GI254023X inhibitor (Figures 5A and 5B, 5B'). Histological examination of H&E stained sections showed that all cell layers of the incisor epithelium were evident in explants cultured with DMSO (Figure 5C). By contrast, the addition of the GI254023X inhibitor had a dramatic effect on the stratum intermedium layer (Figure 5C'), mimicking the phenotype observed in the epithelium of $K14^{Cre/+}$;$Adam10^{fl/fl}$ incisors. Moreover, ALP activity was severely reduced in the GI254023X treated incisors (compare Figures 5D–5D'), thus confirming the absence of stratum intermedium cells.

It is not clear whether Adam10 inhibition in the epithelium of incisors had an irreversible effect on the progenitors of stratum intermedium cells, or if it affected already established cell lines and was thus reversible. To address this question, incisor explants were first cultured *in vitro* for one week in presence of either DMSO or GI254023X, followed by kidney capsule transplantation (Figure 5A). Tissue was harvested one week after the transplantation and processed for histological analyses. H&E stained sections of control explants revealed that all dental epithelial cell layers were clearly defined, with no apparent cellular disorganization (Figures 5E, 5F, 5G, 5H). In contrast, samples treated with GI254023X before transplantation demonstrated severe structural defects at the most anterior part of the incisors, where the whole epithelium was completely disordered and disorganized (Figure 5E', blue asterisk, Figure 5G'). However, examination of the posterior and median parts of the GI254023X treated incisors clearly showed the reappearance of the stratum intermedium layer beneath a well-organized and ordered preameloblast/ameloblast layer (Figures 5F', 5H'), thus indicating that the effects triggered by Adam10 inhibition are reversible. A detachment of these two layers was often observed in the incisors treated with GI254023X before transplantation (Figure 5E'), possibly because the inhibitor was not entirely eliminated and continued to exert a mild effect on the transplanted incisors.

Lineage tracing of *Notch1*-expressing cells show that *Adam10* deletion induces cell fate changes within the stratum intermedium cell layer

We next studied the fate of *Notch1*-expressing cells upon Adam10 abrogation. For this purpose, we used the $Notch1^{CreERT2/+}$;$R26^{mT/mG}$ transgenic mice in which, after 4-OHT induction, *GFP* expression is activated in the *Notch1*-expressing cells. The ability to conditionally mark *Notch1*-expressing cells allows following of the dental epithelial cell lineages associated with *Notch1* expression and establishing its relationship to the continuous growth and regeneration of rodent incisors. Upon 4-OHT induction, Notch1/GFP-positive cells were localized in the inner dental epithelial cells, in agreement with *in situ* hybridization results. *Notch1* is also expressed in the endothelial cells of the dental papilla and dental follicle. One week after 4-OHT induction, GPF staining was localized mainly in the cells of the stratum intermedium (Figures 6A–6D). Interestingly, GFP staining was also sporadically detected in cells of the stellate reticulum and outer enamel epithelium, as well as in ameloblasts (Figure 6D).

We then analyzed the fate of *Notch1* expressing stratum intermedium cells upon blocking Adam10 function. After one day of treatment, we observed single cells from the stratum intermedium invading the ameloblasts layer (Figures 6F–6H). By the fourth day of treatment, we observed large invaginations of the dental epithelium into the mesenchyme (Figures 6E, 6I, 6J). Within these invaginations, numerous Notch1/GFP-positive cells left the stratum intermedium layer and entered the ameloblast layer (Figures 6K-6N).

DISCUSSION

Cell fate specification and differentiation is regulated by the Notch signaling pathway that mediates interactions between neighboring cells via the physical interaction of Notch ligands with Notch receptors (Andersson et al., 2011; Artavanis-Tsakonas et al., 1999; Ho and Artavanis-Tsakonas, 2016; Kopan, 2012). In teeth, Notch signaling is essential for proper enamel formation, a process that requires the close cooperation of the four specific dental epithelial cell types. Indeed, components of the Notch pathway are specifically expressed in these four dental epithelial lineages and their deletion in mice affects both tooth morphology and enamel formation (Mitsiadis et al., 1995, 1998, 2005, 2010). Amelogenesis requires a tightly controlled sequence of cell proliferation, differentiation, extracellular matrix secretion and mineral deposition (Bartlett, 2013; Gordon and Joester, 2015; Zheng et al., 2013). Minor alterations in these processes lead to functionally relevant modifications of the enamel structure (Cantu et al., 2017). Enamel is the highest mineralized tissue in vertebrates and is characterized by a tightly organized structure that

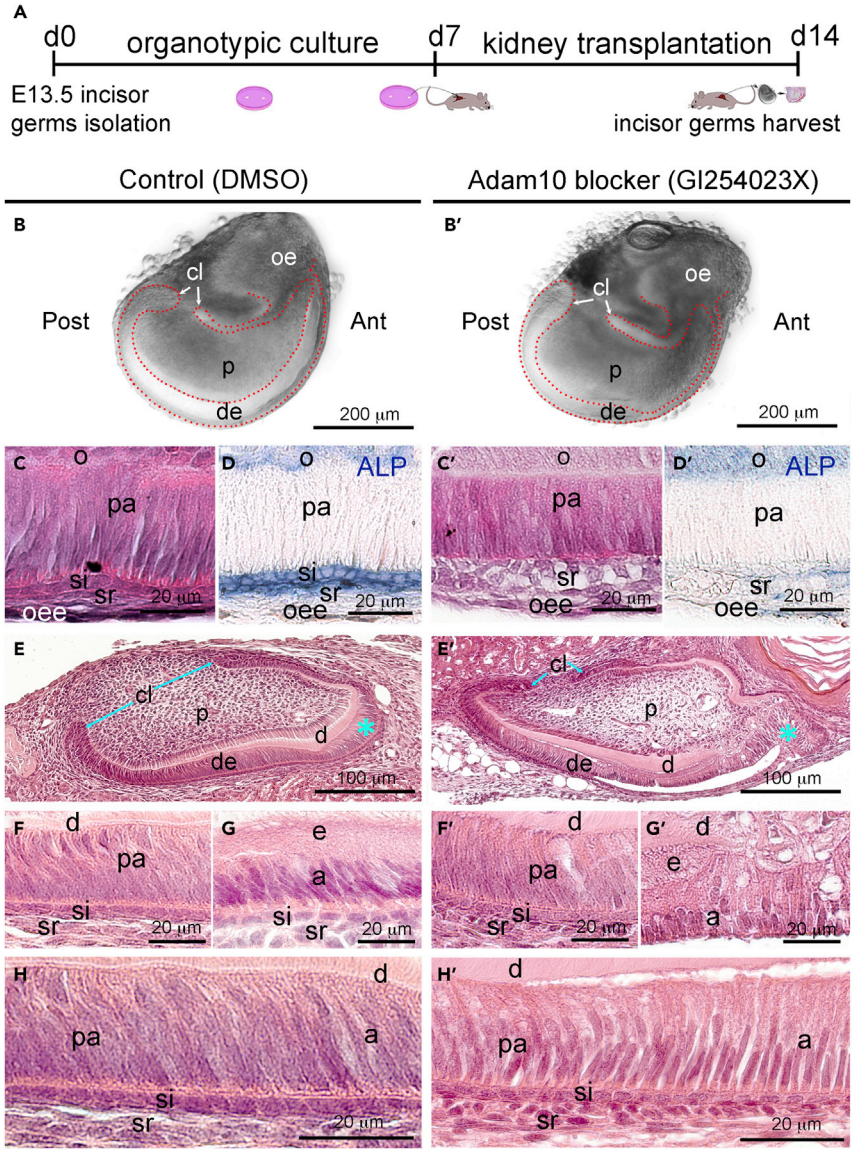

Figure 5. The Adam10 inhibitor GI254023X recapitulates the tooth phenotype induced by genetic deletion of Adam10

(A) Schematic representation of the experimental setup.

(B, B′) Images of E13.5 incisor germs cultured for seven days under control conditions (B) or in presence of GI254023X (B′).

(C-D′) High magnification images of H&E (C, C′) and ALP staining (D, D′) in control (C, D) and GI254023X-treated (C′, D′) incisors, focusing on the differentiated epithelial cell layers, and showing the loss of stratum intermedium (C′) and ALP staining (D′) in GI254023X-treated incisors.

E, E′). H&E staining in control (E) and GI254023X-treated (E′) incisors after kidney capsule transplantation. Asterisks indicate the most anterior (tip) part of the incisors. Notice the disorganized dental epithelium at the anterior part of GI254023X-treated incisors (asterisk in E′).

(F-H′) Higher magnifications of the H&E stained median (F, F′, H, H′) and anterior (G, G′) parts of the control (F, G, H) and GI254023X-treated (F′, G′, H′) incisors. Reestablishment of the ameloblast and stratum intermedium layers at the median part of GI254023X-treated incisors (F′, H′). Absence of stratum intermedium and ameloblasts disorganization in the anterior part of GI254023X-treated incisors (G′). Abbreviations: a, ameloblasts; Ant, anterior part; cl, cervical loop; d, dentine; de, dental epithelium; p, dental pulp; Post, posterior part; e, enamel; o, odontoblasts; oe, oral epithelium; oee, outer enamel epithelium; pa, preameloblasts; si, stratum intermedium; sr, stellate reticulum.

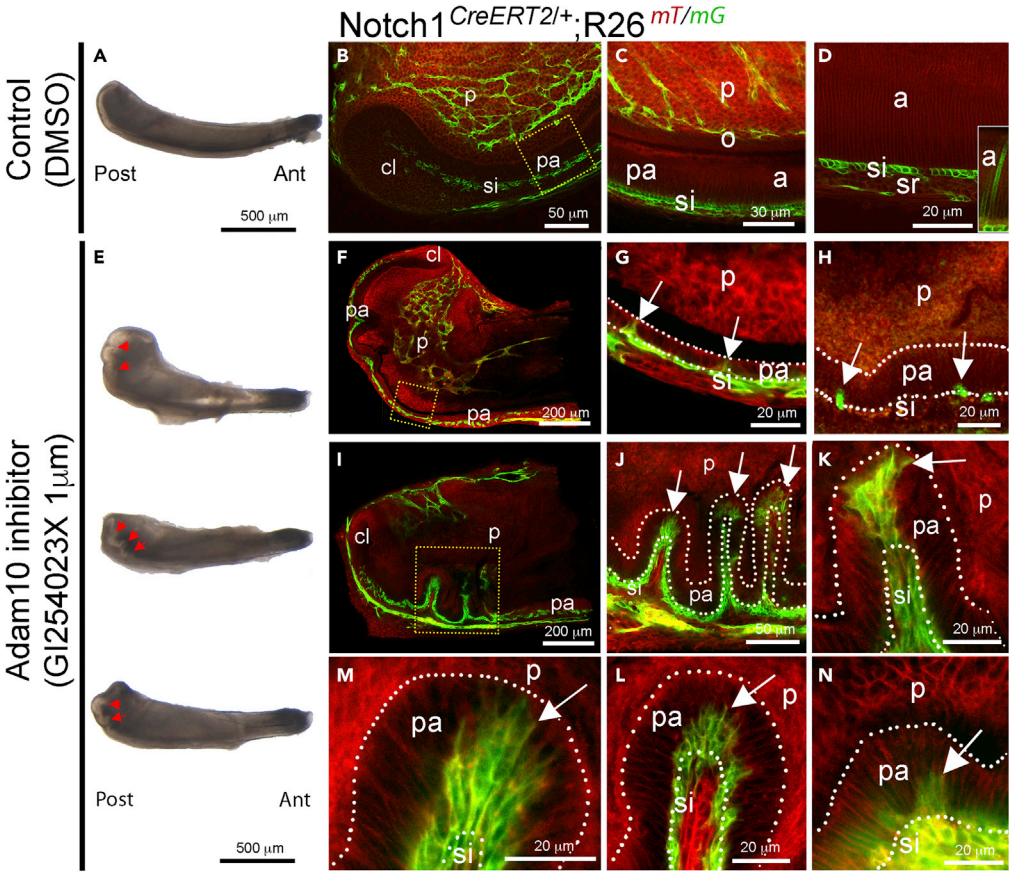

Figure 6. Lineage tracing of *Notch1*-expressing cells upon GI254023X Adam10 inhibition

(A) Brightfield image of the Notch1$^{CreERT2/+}$;R26$^{mT/mG}$ incisor cultured for three days in control conditions.

(B–D) Confocal images showing different regions of the control incisor (A), demonstrating GFP fluorescence in the cuboidal-shaped stratum intermedium cells (B-D) and sporadically in the fully differentiated, elongated ameloblasts (insert in D). Image (C) is high magnification of the yellow dotted area of image (B). White dotted lines indicate the margins of the preameloblast layer from the dental pulp and the stratum intermedium layer.

(E) Notch1$^{CreERT2/+}$;R26$^{mT/mG}$ incisors cultured for one to four days in presence of GI25423X. Red arrows point to the folding areas within the preameloblast layer at the posterior part of the incisors.

(F–H) Confocal images showing GFP fluorescence in the Notch1$^{CreERT2/+}$;R26$^{mT/mG}$ incisors cultured for one day in presence of the inhibitor. Image (G) is high magnification of the yellow dotted area of image (F). White arrows point to GFP-positive cells in the preameloblast layer.

(I–N) Confocal images indicating GFP fluorescent staining in the Notch1$^{CreERT2/+}$;R26$^{mT/mG}$ incisors cultured for four days in presence of the inhibitor. Image (J) is high magnification of the yellow dotted area of image (I) Images (K-N) are high magnifications of the folding areas within the preameloblast layer located at the posterior part of the incisors. White arrows point to the GFP-positive preameloblasts within the folded part of the preameloblast layer. White dotted lines indicate the margins of the preameloblast layer from the dental pulp and the stratum intermedium layer. Abbreviations: a, ameloblasts; Ant, anterior part; cl, cervical loop; e, enamel; o, odontoblasts; p, dental pulp; pa, preameloblasts; Post, posterior part; si, stratum intermedium; sr, stellate reticulum.

provides its exceptional hardness (Gordon et al., 2015). Here we demonstrate that inhibition of Adam10/Notch activity severely affects both the arrangement of the dental epithelium and the structure of enamel. The white and glossy appearance of enamel in the K14$^{Cre/+}$;Adam10$^{fl/fl}$ incisors is indicative of important enamel alterations such as enamel hypoplasia, hypomaturation and hypomineralization (Mitsiadis and Luder, 2011).

Detailed histological analyses of the K14$^{Cre/+}$;Adam10$^{fl/fl}$ incisors show disappearance of a stratum intermedium as a distinct layer of cuboidal cells and a widespread disorder of the ameloblast and stellate reticulum layers that occurs concomitantly with initiation of mineral matrix deposition. Absence of stratum

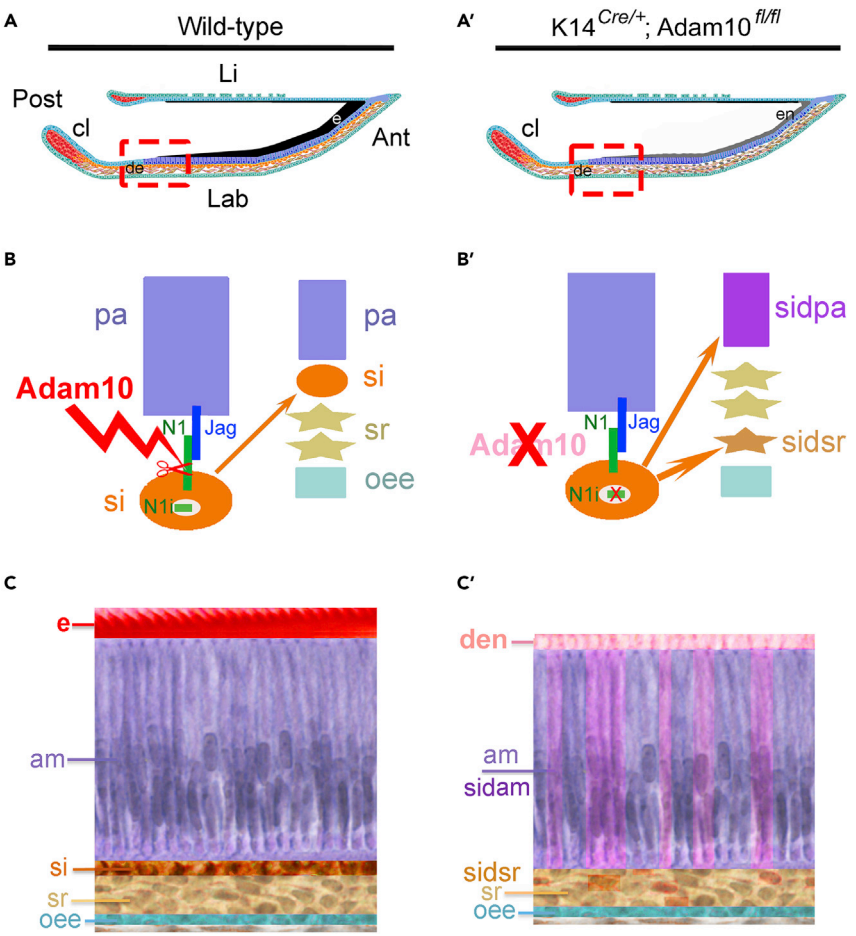

Figure 7. Hypothetical model illustrating the function of Adam10 in the mouse incisor

(A, A′) Schematic representation of wild-type (A) and K14$^{Cre/+}$;Adam10$^{fl/fl}$ (A′) incisors showing the absence of stratum intermedium and the deposition of a dysfunctional enamel upon Adam10 deletion. Red dashed boxes indicate the areas where stratum intermedium cell fate change starts and the stratum intermedium cells adopt the preameloblast and stellate reticulum cell fates in the K14$^{Cre/+}$;Adam10$^{fl/fl}$ incisors (A′).

(B, B′) Schematic representation of the mechanism of Adam10 action in the dental epithelium. Adam10 is responsible for the cleavage of Notch1 in stratum intermedium cells (red scissors) that enables nuclear translocation of the Notch1 intracellular domain (B; Notch1i, in green). Depletion of Adam10 in the incisor epithelium disables nuclear translocation of the Notch1 intracellular domain, thus deregulating the function of the Notch pathway. This initiates conversion of a portion of stratum intermedium cells into preameloblasts and consequent ameloblast disorganization and impaired enamel formation. In addition, another portion of stratum intermedium cells flattens and becomes stellate reticulum cells participating in the formation of the incisor's papillary cell layer.

(C, C′) Cartoon depicting the definitive alterations in the number and composition of the epithelial cell layers (each of them represented by a specific color) and enamel formation in the K14$^{Cre/+}$;Adam10$^{fl/fl}$ incisors. Stratum intermedium (orange color) cell fate change toward the stellate reticulum and preameloblast/ameloblast fate generates the additional stratum intermedium-derived stellate reticulum (enhanced brown color) and stratum intermedium-derived ameloblasts (enhanced violet color) and leads to defective enamel deposition. Abbreviations: am, ameloblasts; Ant, anterior part; cl, cervical loop; de, dental epithelium; den, dysfunctional enamel; e, enamel; Jag, Jagged; Lab, labial side; Li, lingual side; N1, Notch1; N1i, intracellular Notch1; oee, outer enamel epithelium; pa, preameloblasts; Post, posterior part; si, stratum intermedium; sidam, stratum intermedium-derived ameloblasts; sidpa, stratum intermedium-derived preameloblasts; sr, stellate reticulum.

intermedium cells is not associated with apoptotic events, which suggests that inactivation of Adam10 affects their fate and misroutes these cells into alternative developmental pathways, either as ameloblasts or stellate reticulum cells (Figure 7). Increasing the number of one specialized cell type at the expense of another inevitably leads to changes in cell organization and composition, as well as in the enamel structure.

The apparent enamel defects and enamel deposition in ectopic sites in the Adam10 mutants are linked with extreme disorganization and disorientation of ameloblasts. Similar deformations, including defects in bristle shaft, irregular bristle polarity and abnormal deposition of lens material, have been observed in *Drosophila* eyes upon Notch signaling deregulation (Das et al., 2013; Fortini and Artavanis-Tsakonas, 1994).

The K14$^{Cre/+}$;Adam10$^{fl/fl}$ incisors demonstrate increased number of ameloblasts, due to increased proliferative activity of preameloblasts and the fate change of stratum intermedium cells. A strict balance between the number of ameloblasts and the space they occupy exists in the wild-type incisors. In K14$^{Cre/+}$;Adam10$^{fl/fl}$ incisors, however, this equilibrium is disturbed by the increased number of ameloblasts, thus resulting in the folding and further disorganization of the ameloblast layer. Consequently, the ameloblasts in K14$^{Cre/+}$;Adam10$^{fl/fl}$ incisors are characterized by loss of polarity, as indicated by the ectopic secretion of enamel at their basal end, and defective differentiation, characterized by the ectopic expression of Notch2 and K14. Of importance, these changes are not caused by a loss of Adam10 activity in ameloblasts because exclusive deletion of Adam10 in ameloblasts, and consequently enamel, of Amelx$^{Cre/+}$;Adam10$^{fl/fl}$ incisors had no effect neither on organization and morphology of ameloblast layer nor enamel structure.

Although the function and the roles of ameloblasts in the process of enamel formation in the continuously growing incisors are well established (Bartlett, 2013; Mitsiadis and Graf, 2009), fewer information exists for the other three dental epithelial cell types. For example, it is not yet known when the fate of these various cell types is established. A number of studies suggested that the ameloblasts and stratum intermedium share a common progenitor in transit-amplifying cells (Harada et al., 1999, 2006; Sharir et al., 2019), and recently outer dental epithelium progenitors were identified by scRNA-seq (Krivanek et al., 2020). The current notion is that the stem cells responsible for the generation of all dental epithelial cell lineages reside in the cervical loop of the incisor (Juuri et al., 2012; Krivanek et al., 2020; Li et al., 2012; Mitsiadis et al., 2007; Sharir et al., 2019). Our findings suggest that the fate determination of these cells is more flexible and is regulated by the Adam10/Notch axis. Previous studies suggested that Notch signaling induces the divergence of the stratum intermedium from the ameloblast lineage (Harada et al., 2006). Recently, we showed that *Notch1* expressing cells of the stratum intermedium represent progenitor cells that are activated upon injury and regenerate the ameloblast layer (Sharir et al., 2019). The persisting *Notch1* expression in the posterior part of K14$^{Cre/+}$;Adam10$^{fl/fl}$ incisors suggests the presence of stratum intermedium precursors in these teeth.

Here we show that the absence of stratum intermedium generates a less refined and organized enamel structure resembling to the enameloid of lower vertebrates such as sharks (Fraser et al., 2013; Kawasaki et al., 2021; Smith et al., 2015; Wilmers et al., 2021). We have previously shown that K14$^{Cre/+}$;*Jagged2*$^{fl/fl}$ mice display aberrant tooth morphology, disorganization of the epithelium and altered enamel formation and structure (Mitsiadis et al., 2005, 2010). Other studies, where Notch signaling was pharmacologically inhibited postnatally, demonstrated absence of a direct effect on ameloblasts (Jheon et al., 2016). However, contacts between ameloblasts and stratum intermedium cells were disrupted, which eventually led to enamel defects (Jheon et al., 2016). Similarly, our analyses of K14$^{Cre/+}$;Adam10$^{fl/fl}$ incisors showed an irregular stratum intermedium, with territories of both detachment from the ameloblast layer and ectopic formation of cell clusters whereas the overall organization of the ameloblast layer was not affected. Therefore, Notch signaling deregulation within the dental epithelium does not allow cell lineages to maintain their specific molecular print, which is important for their cellular specificity and function. The tooth enamel phenotype shows a direct effect of Adam10 on the ability to generate signals linked to Notch1 activation for the maintenance of stratum intermedium and overall dental epithelial architecture. Our results nevertheless indicate that Adam10 activity is necessary to maintain *Notch1*-expressing cells identity as stratum intermedium cells. These cells are multipotent and can acquire the ameloblast fate upon injury, as we recently demonstrated (Sharir et al., 2019). This injury-dependent cell fate switch is homologous to the one induced by Adam10 inhibition, which thus suggests that modulation of Adam10 activity could be a mechanism underlying the recruitment of stratum intermedium cells upon injury. Hence, Adam10 deletion likely causes switch of early Notch1 expressing progenitors to cells of the inner enamel epithelium/preameloblast layer instead of the stratum intermedium layer. However, we cannot exclude the possibility that Adam10 deletion might induce the conversion of some stratum intermedium cells to preameloblasts via inhibition of the Notch signaling pathway, although our data do not provide a direct evidence of this conversion. Although the phenotype clearly highlights the role of Adam10 in Notch1 signaling, we cannot exclude the possibility that the reduced shedding of other Adam10 targets, which include important adhesion molecules (Wetzel et al., 2017), could partly contribute to these severe abnormalities.

Taken together, our results show that Adam10 exerts a fundamental role in preserving Notch-dependent cell identity in dental epithelial cells, and the establishment of the four distinct dental epithelial cell populations that orchestrate the generation and proper composition of enamel.

Limitations of the study

In this work, we demonstrate that *Adam10* deletion leads to loss of stratum intermedium cells due to their switch toward the ameloblast lineage. We propose that this event induces depolarization of ameloblasts and overcrowding of the ameloblast layer, which in turn causes the formation of defective enamel. Although this would be the most logical and simple explanation, it is challenging to obtain a full, mechanistic dissection of these series of events. We further demonstrate that Adam10 deletion is accompanied by loss of *Notch1*-expressing stratum intermedium cells, and our lineage tracing experiments strongly support a fate switch of these cells toward the ameloblast lineage. Nevertheless, our data do not provide direct evidence of this conversion.

STAR★METHODS

Detailed methods are provided in the online version of this paper and include the following:

- KEY RESOURCES TABLE
- RESOURCE AVAILABILITY
  - Lead contact
  - Materials availability
  - Data and code availability
- EXPERIMENTAL MODEL AND SUBJECT DETAILS
  - Animals
- METHOD DETAILS
  - Tissue isolation and preparation
  - Microcomputed tomography (μCT)
  - Scanning Electron Microscopy (SEM) evaluation and Toluidine Blue staining
  - Transmission Electron Microscopy (TEM)
  - Histological evaluation
  - Orientation analysis of ameloblasts
  - *In situ* hybridization
  - Immunostaining and immunofluorescence on sections and as whole mount
  - Terminal deoxynucleotidyl transferase-mediated dUTP nick end labeling (TUNEL)
  - *In vitro* and *ex vivo* cultures of embryonic and postnatal incisors
  - Alkaline Phosphatase (ALP) activity
- QUANTIFICATION AND STATISTICAL ANALYSIS

SUPPLEMENTAL INFORMATION

Supplemental information can be found online at https://doi.org/10.1016/j.isci.2022.105154.

ACKNOWLEDGMENTS

We wish to thank Prof. Yufang Zheng (School of Life Sciences, Fudan University, Shanghai, China) for providing the *Adam10* probe, Dr Yoshihiko Yamada (Laboratory of Cell and Developmental Biology, National Institute of Dental and Craniofacial Research, National Institutes of Health, Bethesda, Maryland, USA) for providing the *Ambn* probe and Prof. Andreas Ludwig (Institute for Biochemistry, Christian Albrechts University, Kiel, Germany) for providing the GI254023X chemical. We are thankful to Prof. Alexander Tsouknidas (Department of Mechanical Engineering, University of Western Macedonia, Greece) for computational image analysis. This work has been supported by institutional funds from the University of Zurich (UZH) and the Deutsche Forschungsgemeinschaft (SFB877-A3).

AUTHOR CONTRIBUTIONS

Conceptualization, T.A.M; Methodology, T.A.M., L.J.R., and P.P.; Validation, L.J.R., P.P., T.A.M., P.S., and S.W.; Formal analysis, T,A.M., L.J.R., A.B., and P.P.; Investigation, T.A.M., L.J.R., and P.P.; Resources, T.A.M., P.S., and S.W.; Data curation, T.A.M., L.J.R., A.B., and P.P.; Writing – original draft, T.A.M., P.P.,

and L.J.R.; Writing – Review and Editing, T.A.M., A.B., P.P., and L.J.R.; Visualization, T.A.M., P.P., L.J.R., and P.P.; Supervision, T.A.M.; Project administration: T.A.M.; Funding acquisition, T.A.M.

DECLARATION OF INTERESTS

The authors have no conflicts of interest to report.

Received: April 20, 2022
Revised: June 27, 2022
Accepted: September 14, 2022
Published: October 21, 2022

REFERENCES

Andersson, E.R., Sandberg, R., and Lendahl, U. (2011). Notch signaling: simplicity in design, versatility in function. Development *138*, 3593–3612.

Artavanis-Tsakonas, S., Matsuno, K., and Fortini, M.E. (1995). Notch signaling. Science *268*, 225–232.

Artavanis-Tsakonas, S., and Muskavitch, M.A.T. (2010). Notch: the past, the present, and the future. Curr. Top. Dev. Biol. *92*, 1–29.

Artavanis-Tsakonas, S., Rand, M.D., and Lake, R.J. (1999). Notch signaling: cell fate control and signal integration in development. Science *284*, 770–776.

Balic, A., and Thesleff, I. (2015). Tissue interactions regulating tooth development and renewal. Curr. Top. Dev. Biol. *115*, 157–186.

Bartlett, J.D. (2013). Dental enamel development: proteinases and their enamel matrix substrates. ISRN Dent. *2013*, 684607.

Cantù, C., Pagella, P., Shajiei, T.D., Zimmerli, D., Valenta, T., Hausmann, G., Basler, K., and Mitsiadis, T.A. (2017). A cytoplasmic role of Wnt/beta-catenin transcriptional cofactors Bcl9, Bcl9l, and Pygopus in tooth enamel formation. Sci. Signal. *10*, eaah4598.

Cobourne, M.T., and Mitsiadis, T. (2006). Neural crest cells and patterning of the mammalian dentition. J. Exp. Zool. B Mol. Dev. Evol. *306*, 251–260.

Das, S., Chen, Q.B., Saucier, J.D., Drescher, B., Zong, Y., Morgan, S., Forstall, J., Meriwether, A., Toranzo, R., and Leal, S.M. (2013). The Drosophila T-box transcription factor Midline functions within the Notch-Delta signaling pathway to specify sensory organ precursor cell fates and regulates cell survival within the eye imaginal disc. Mech. Dev. *130*, 577–601.

Felasa Working Group On Farm Animals Corina Mihaela Berset Convenor, Caristo, M.E., Ferrara, F., Hardy, P., Oropeza-Moe, M., and Waters, R. (2021). Federation of European Laboratory Animal Science Associations recommendations of best practices for the health management of ruminants and pigs used for scientific and educational purposes. Lab. Anim. *55*, 117–128.

Fleming, R.J., Purcell, K., and Artavanis-Tsakonas, S. (1997). The NOTCH receptor and its ligands. Trends Cell Biol. *7*, 437–441.

Fortini, M.E., and Artavanis-Tsakonas, S. (1994). The suppressor of hairless protein participates in notch receptor signaling. Cell *79*, 273–282.

Fraser, G.J., Bloomquist, R.F., and Streelman, J.T. (2013). Common developmental pathways link tooth shape to regeneration. Dev. Biol. *377*, 399–414.

Fre, S., Hannezo, E., Sale, S., Huyghe, M., Lafkas, D., Kissel, H., Louvi, A., Greve, J., Louvard, D., and Artavanis-Tsakonas, S. (2011). Notch lineages and activity in intestinal stem cells determined by a new set of knock-in mice. PLoS One *6*, e25785.

Gordon, L.M., Cohen, M.J., MacRenaris, K.W., Pasteris, J.D., Seda, T., and Joester, D. (2015). Dental materials. Amorphous intergranular phases control the properties of rodent tooth enamel. Science *347*, 746–750.

Gordon, L.M., and Joester, D. (2015). Mapping residual organics and carbonate at grain boundaries and the amorphous interphase in mouse incisor enamel. Front. Physiol. *6*, 57.

Gray, G.E., Mann, R.S., Mitsiadis, E., Henrique, D., Carcangiu, M.L., Banks, A., Leiman, J., Ward, D., Ish-Horowitz, D., and Artavanis-Tsakonas, S. (1999). Human ligands of the Notch receptor. Am. J. Pathol. *154*, 785–794.

Guruharsha, K.G., Kankel, M.W., and Artavanis-Tsakonas, S. (2012). The Notch signalling system: recent insights into the complexity of a conserved pathway. Nat. Rev. Genet. *13*, 654–666.

Harada, H., Ichimori, Y., Yokohama-Tamaki, T., Ohshima, H., Kawano, S., Katsube, K.i., and Wakisaka, S. (2006). Stratum intermedium lineage diverges from ameloblast lineage via Notch signaling. Biochem. Biophys. Res. Commun. *340*, 611–616.

Harada, H., Kettunen, P., Jung, H.S., Mustonen, T., Wang, Y.A., and Thesleff, I. (1999). Localization of putative stem cells in dental epithelium and their association with Notch and FGF signaling. J. Cell Biol. *147*, 105–120.

Ho, D.M., and Artavanis-Tsakonas, S. (2016). The notch-mediated proliferation circuitry. Curr. Top. Dev. Biol. *116*, 17–33.

Hoettecke, N., Ludwig, A., Foro, S., and Schmidt, B. (2010). Improved synthesis of ADAM10 inhibitor GI254023X. Neurodegener. Dis. *7*, 232–238.

Hori, K., Sen, A., and Artavanis-Tsakonas, S. (2013). Notch signaling at a glance. J. Cell Sci. *126*, 2135–2140.

Ikeda, A., Shahid, S., Blumberg, B.R., Suzuki, M., and Bartlett, J.D. (2019). ADAM10 is expressed by ameloblasts, cleaves the RELT TNF receptor extracellular domain and Facilitates enamel development. Sci. Rep. *9*, 14086.

Inoshima, N., Wang, Y., and Bubeck Wardenburg, J. (2012). Genetic requirement for ADAM10 in severe Staphylococcus aureus skin infection. J. Invest. Dermatol. *132*, 1513–1516.

Jheon, A.H., Prochazkova, M., Meng, B., Wen, T., Lim, Y.J., Naveau, A., Espinoza, R., Cox, T.C., Sone, E.D., Ganss, B., et al. (2016). Inhibition of notch signaling during mouse incisor renewal leads to enamel defects. J. Bone Miner. Res. *31*, 152–162.

Jimenez-Rojo, L., and Mitsiadis, T.A. (2019). Tissue recombination and kidney capsule transplantation assays for the study of epithelial-mesenchymal interactions. Methods Mol. Biol. *1922*, 49–55.

Jorissen, E., Prox, J., Bernreuther, C., Weber, S., Schwanbeck, R., Serneels, L., Snellinx, A., Craessaerts, K., Thathiah, A., Tesseur, I., et al. (2010). The disintegrin/metalloproteinase ADAM10 is essential for the establishment of the brain cortex. J. Neurosci. *30*, 4833–4844.

Juuri, E., Saito, K., Ahtiainen, L., Seidel, K., Tummers, M., Hochedlinger, K., Klein, O.D., Thesleff, I., and Michon, F. (2012). Sox2+ stem cells contribute to all epithelial lineages of the tooth via Sfrp5+ progenitors. Dev. Cell *23*, 317–328.

Kaplan, N., Ventrella, R., Peng, H., Pal-Ghosh, S., Arvanitis, C., Rappoport, J.Z., Mitchell, B.J., Stepp, M.A., Lavker, R.M., and Getsios, S. (2018). EphA2/Ephrin-A1 mediate corneal epithelial cell compartmentalization via ADAM10 regulation of EGFR signaling. Invest. Ophthalmol. Vis. Sci. *59*, 393–406.

Kawasaki, K., Keating, J.N., Nakatomi, M., Welten, M., Mikami, M., Sasagawa, I., Puttick, M.N., Donoghue, P.C.J., and Ishiyama, M. (2021). Coevolution of enamel, ganoin, enameloid, and their matrix SCPP genes in osteichthyans. iScience *24*, 102023.

Kopan, R. (2012). Notch signaling. Cold Spring Harb. Perspect. Biol. *4*, a011213.

Kopan, R., and Ilagan, M.X.G. (2009). The canonical Notch signaling pathway: unfolding the activation mechanism. Cell *137*, 216–233.

Kovall, R.A., Gebelein, B., Sprinzak, D., and Kopan, R. (2017). The canonical notch signaling pathway: structural and biochemical insights into shape, sugar, and Force. Dev. Cell *41*, 228–241.

Krivanek, J., Soldatov, R.A., Kastriti, M.E., Chontorotzea, T., Herdina, A.N., Petersen, J., Szarowska, B., Landova, M., Matejova, V.K., Holla, L.I., et al. (2020). Dental cell type atlas reveals stem and differentiated cell types in mouse and human teeth. Nat. Commun. *11*, 4816.

Lambrecht, B.N., Vanderkerken, M., and Hammad, H. (2018). The emerging role of ADAM metalloproteinases in immunity. Nat. Rev. Immunol. *18*, 745–758.

Larsson, A. (1976). Histochemical localization of alkaline pyrophosphate- phosphohydrolase in tooth-forming cells of rat. Scand. J. Dent. Res. *84*, 63–75.

Li, C.Y., Cha, W., Luder, H.U., Charles, R.P., McMahon, M., Mitsiadis, T.A., and Klein, O.D. (2012). E-cadherin regulates the behavior and fate of epithelial stem cells and their progeny in the mouse incisor. Dev. Biol. *366*, 357–366.

Luder, H.U., and Amstad-Jossi, M. (2012). Electron microscopy. Methods Mol. Biol. *887*, 81–93.

Ludwig, A., Hundhausen, C., Lambert, M.H., Broadway, N., Andrews, R.C., Bickett, D.M., Leesnitzer, M.A., and Becherer, J.D. (2005). Metalloproteinase inhibitors for the disintegrin-like metalloproteinases ADAM10 and ADAM17 that differentially block constitutive and phorbol ester-inducible shedding of cell surface molecules. Comb. Chem. High Throughput Screen. *8*, 161–171.

Mitsiadis, T.A., Barrandon, O., Rochat, A., Barrandon, Y., and De Bari, C. (2007). Stem cell niches in mammals. Exp. Cell Res. *313*, 3377–3385.

Mitsiadis, T.A., and Graf, D. (2009). Cell fate determination during tooth development and regeneration. Birth Defects Res. C Embryo Today. *87*, 199–211.

Mitsiadis, T.A., Graf, D., Luder, H., Gridley, T., and Bluteau, G. (2010). BMPs and FGFs target Notch signalling via jagged 2 to regulate tooth morphogenesis and cytodifferentiation. Development *137*, 3025–3035.

Mitsiadis, T.A., Henrique, D., Thesleff, I., and Lendahl, U. (1997). Mouse Serrate-1 (Jagged-1): expression in the developing tooth is regulated by epithelial-mesenchymal interactions and fibroblast growth factor-4. Development *124*, 1473–1483.

Mitsiadis, T.A., Hirsinger, E., Lendahl, U., and Goridis, C. (1998). Delta-notch signaling in odontogenesis: correlation with cytodifferentiation and evidence for feedback regulation. Dev. Biol. *204*, 420–431.

Mitsiadis, T.A., Lardelli, M., Lendahl, U., and Thesleff, I. (1995). Expression of Notch 1, 2 and 3 is regulated by epithelial-mesenchymal interactions and retinoic acid in the developing mouse tooth and associated with determination of ameloblast cell fate. J. Cell Biol. *130*, 407–418.

Mitsiadis, T.A., and Luder, H.U. (2011). Genetic basis for tooth malformations: from mice to men and back again. Clin. Genet. *80*, 319–329.

Mitsiadis, T.A., Regaudiat, L., and Gridley, T. (2005). Role of the Notch signalling pathway in tooth morphogenesis. Arch. Oral Biol. *50*, 137–140.

Mizuno, S., Yoda, M., Kimura, T., Shimoda, M., Akiyama, H., Chiba, K., Nakamura, M., and Horiuchi, K. (2020). ADAM10 is indispensable for longitudinal bone growth in mice. Bone *134*, 115273.

Mizuno, S., Yoda, M., Shimoda, M., Chiba, K., Nakamura, M., and Horiuchi, K. (2018). Inhibition of ADAM10 in satellite cells accelerates muscle regeneration following muscle injury. J. Orthop. Res. *36*, 2259–2265.

Nye, J.S., and Kopan, R. (1995). Developmental signaling. Vertebrate ligands for Notch. Curr. Biol. *5*, 966–969.

Pagella, P., Porcheri, C., and Mitsiadis, T.A. (2020). Exploiting teeth as a model to study basic features of signaling pathways. Biochem. Soc. Trans. *48*, 2729–2742.

Said, R., Zheng, L., Saunders, T., Zeidler, M., Papagerakis, S., and Papagerakis, P. (2019). Generation of amelx-iCre mice supports ameloblast-specific role for Stim1. J. Dent. Res. *98*, 1002–1010.

Sakamoto, K., Jin, S.P., Goel, S., Jo, J.H., Voisin, B., Kim, D., Nadella, V., Liang, H., Kobayashi, T., Huang, X., et al. (2021). Disruption of the endopeptidase ADAM10-Notch signaling axis leads to skin dysbiosis and innate lymphoid cell-mediated hair follicle destruction. Immunity *54*, 2321–2337.e10.

Schindelin, J., Arganda-Carreras, I., Frise, E., Kaynig, V., Longair, M., Pietzsch, T., Preibisch, S., Rueden, C., Saalfeld, S., Schmid, B., et al. (2012). Fiji: an open-source platform for biological-image analysis. Nat. Methods *9*, 676–682.

Sharir, A., Marangoni, P., Zilionis, R., Wan, M., Wald, T., Hu, J.K., Kawaguchi, K., Castillo-Azofeifa, D., Epstein, L., Harrington, K., et al. (2019). A large pool of actively cycling progenitors orchestrates self-renewal and injury repair of an ectodermal appendage. Nat. Cell Biol. *21*, 1102–1112.

Siebel, C., and Lendahl, U. (2017). Notch signaling in development, tissue homeostasis, and disease. Physiol. Rev. *97*, 1235–1294.

Smith, C.E., and Nanci, A. (1995). Overview of morphological changes in enamel organ cells associated with major events in amelogenesis. Int. J. Dev. Biol. *39*, 153–161.

Smith, M.M., Johanson, Z., Butts, T., Ericsson, R., Modrell, M., Tulenko, F.J., Davis, M.C., and Fraser, G.J. (2015). Making teeth to order: conserved genes reveal an ancient molecular pattern in paddlefish (Actinopterygii). Proc. Biol. Sci. *282*, 20142700.

Solanas, G., Cortina, C., Sevillano, M., and Batlle, E. (2011). Cleavage of E-cadherin by ADAM10 mediates epithelial cell sorting downstream of EphB signalling. Nat. Cell Biol. *13*, 1100–1107.

Tsai, Y.H., VanDussen, K.L., Sawey, E.T., Wade, A.W., Kasper, C., Rakshit, S., Bhatt, R.G., Stoeck, A., Maillard, I., Crawford, H.C., et al. (2014). ADAM10 regulates Notch function in intestinal stem cells of mice. Gastroenterology *147*, 822–834.e13.

Weber, S., Niessen, M.T., Prox, J., Lüllmann-Rauch, R., Schmitz, A., Schwanbeck, R., Blobel, C.P., Jorissen, E., de Strooper, B., Niessen, C.M., and Saftig, P. (2011). The disintegrin/metalloproteinase Adam10 is essential for epidermal integrity and Notch-mediated signaling. Development *138*, 495–505.

Weber, S., and Saftig, P. (2012). Ectodomain shedding and ADAMs in development. Development *139*, 3693–3709.

Wetzel, S., Seipold, L., and Saftig, P. (2017). The metalloproteinase ADAM10: a useful therapeutic target? Biochim. Biophys. Acta. Mol. Cell Res. *1864*, 2071–2081.

Wilmers, J., Waldron, M., and Bargmann, S. (2021). Hierarchical microstructure of tooth enameloid in two lamniform shark species, carcharias taurus and Isurus oxyrinchus. Nanomaterials *11*.

Yu, T., and Klein, O.D. (2020). Molecular and cellular mechanisms of tooth development, homeostasis and repair. Development *147*.

Zheng, L., Seon, Y.J., Mourão, M.A., Schnell, S., Kim, D., Harada, H., Papagerakis, S., and Papagerakis, P. (2013). Circadian rhythms regulate amelogenesis. Bone *55*, 158–165.

STAR★METHODS

KEY RESOURCES TABLE

.

REAGENT or RESOURCE	SOURCE	IDENTIFIER
Antibodies		
Rabbit polyclonal anti-Amelogenin	Abcam	Cat#ab59705
Rat monoclonal anti-Adam10	R&D Systems	Cat#mab946
Rabbit polyclonal anti-Keratin 14	BioLegend (prev. Covance)	Cat#905301 (prev. PRB-155P-100)
Rabbit polyclonal anti-Notch1	Mitsiadis et al., (1995)	N/A
Rabbit polyclonal anti-Notch2	Mitsiadis et al., (1995)	N/A
Rabbit polyclonal anti-Phospho-Histone3	Santa Cruz	Cat# sc-8656-R
Donkey anti-Rabbit IgG (H + L) Highly Cross-Adsorbed Secondary Antibody, Alexa Fluor™ 488	Invitrogen/ThermoFisher Scientific	Cat#A21206
Donkey anti-Rat IgG (H + L) Highly Cross-Adsorbed Secondary Antibody, Alexa Fluor™ 568	Invitrogen/ThermoFisher Scientific	Cat# A78946
Chemicals, peptides, and recombinant proteins		
Focus Clear©	CelExplorer	Cat#FC-101
GI254023X	Sigma-Aldrich	Cat# SML0789
4-hydroxytamoxifen (4-OHT)	Sigma-Aldrich	Cat#H7904
Experimental models: Organisms/strains		
Mouse strain: Adam10$^{fl/fl}$	Jorissen et al., (2010)	MGI: 4838238
Mouse strain: Keratin14-Cre (K14$^{Cre/+}$)	The Jackson Laboratory	MGI: 2445832
Mouse strain: R26$^{mT/mG}$	The Jackson Laboratory	MGI: 3716464
Mouse strain: Notch1-CreERT2^{SAT} (Notch1$^{CreERT2/+}$)	Fre et al., (2011)	MGI: 5304912
Oligonucleotides		
Riboprobe anti-Notch1	Mitsiadis et al., (1995), 1998	N/A
Riboprobe anti-Notch2	Mitsiadis et al., (1995), 1998	N/A
Riboprobe anti-Adam10	Gift from Prof. Yufang Zheng	N/A
Riboprobe anti-Ameloblastin	Gift from Dr. Yoshihiko Yamada	N/A
Software and algorithms		
VGStudio MAX 2.0	Volume Graphics GMBH	https://www.volumegraphics.com/en/products/vgsm.html
Imaris 9.0	Bitplane	https://imaris.oxinst.com/versions/9
Fiji	Schindelin et al., (2012)	https://imagej.net/software/fiji/

RESOURCE AVAILABILITY

Lead contact

Information and requests for resources and reagents should be directed to and will be fulfilled by the lead contact, Thimios A. Mitsiadis (thimios.mitsiadis@zzm.uzh.ch).

Materials availability

This study did not generate new unique reagents.

Data and code availability

Data reported in this paper will be shared by the lead contact on request. This paper does not report original code.

EXPERIMENTAL MODEL AND SUBJECT DETAILS

Animals

All mice were maintained and handled according to the Swiss Animal Welfare Law and in compliance with the regulations of the Cantonal Veterinary office, Zurich (License for animal experimentation ZH15½014; ZH146/17; ZH018/17). The animal facility provided standardized housing conditions, with a mean room temperature of 21 ± 1°C, 50% ± 5% humidity, and 15 complete changes of filtered air per hour (HEPA H 14filter); air pressure was controlled at 50 Pa. The light/dark cycle in the animal rooms was set to a 12 h/12 h cycle (lights on at 07:00, lights off at 19:00) with artificial light of approximately 40 Lux in the cage. The animals had unrestricted access to sterilized drinking water, and *ad libitum* access to a pelleted and extruded mouse diet in the food hopper (Kliba No. 3436; Provimi Kliba/Granovit AG, Kaiseraugst, Switzerland). Mice were housed in a barrier-protected specific pathogen-free unit and were kept in groups of max. 5 adult mice per cage in standard IVC cages (Allentown Mouse 500; 194 × 181 × 398 mm, floor area 500 cm2; Allentown, NJ, USA) with autoclaved dust-free poplar bedding (JRS GmbH + Co KG, Rosenberg, Germany). A standard cardboard house (Ketchum Manufacturing, Brockville, Canada) served as a shelter, and tissue papers were provided as nesting material. In addition, crinklets (SAFE crinklets natural, JRS GmbH + Co KG, Rosenberg, Germany) were provided as enrichment and further nesting material. The specific pathogen-free status of the animals was monitored frequently and confirmed according to FELASA guidelines by a sentinel program. The mice were free of all viral, bacterial, and parasitic pathogens listed in FELASA recommendations (Felasa Working Group On Farm Animals Corina Mihaela Berset Convenor et al., 2021).

To study the effect of Adam10 deletion in the dental epithelium, Adam10$^{fl/fl}$ (MGI: 4838238) mice (Jorissen et al., 2010) were crossed with Keratin14-Cre (K14$^{Cre/+}$) (MGI: 2445832) and R26$^{mT/mG}$ (MGI: 3716464) mice (The Jackson Laboratory). Homozygous Adam10$^{fl/fl}$;R26$^{mT/mG}$ mice were crossed with K14$^{Cre/+}$;Adam10$^{fl/+}$ mice. Conditional K14$^{Cre/+}$;Adam10$^{fl/fl}$ knockout mice were harvested for analysis at different developmental points, as detailed in the "Method details" section and in the figure legends. Littermates of Adam10$^{fl/+}$ mice were used as controls. To trace *Notch1* expressing cells, Notch1-CreERT2^{SAT} (Notch1$^{CreERT2/+}$; MGI: 5304912) mice (Fre et al., 2011) were crossed with R26$^{mT/mG}$ mice to obtain Notch1$^{CreERT2/+}$;R26$^{mT/mG}$ mice. To assess the effects of the deletion of Adam10 specifically in ameloblasts, we crossed Amelx$^{Cre/+}$ mice (Said et al., 2019) (a gift from Professor Petros Papagerakis) with Adam10$^{fl/fl}$ mice and R26$^{mT/mG}$ mice. At least 3 biological replicates were used for each experiment, unless differently indicated. Animals were allocated to experimental groups based on their genotype; animals of different sex were randomly allocated.

METHOD DETAILS

Tissue isolation and preparation

Tissues used in this study were harvested at different stages ranging from embryonic day 13.5 (E13.5) to postnatal day 19 (P19). Experiments at postnatal stages involving the K14$^{Cre/+}$;Adam10$^{fl/fl}$ mice were mainly performed on P1-P2 incisors because only very few mutant pups survived after this age, as previously reported (Weber et al., 2011). Mouse embryos were sacrificed by decapitation and heads were fixed in 4% paraformaldehyde (PFA) overnight at 4°C. Endocardial perfusion with 4% PFA was performed in pups, after which the heads were harvested and further fixed in 4% PFA overnight at 4°C. The heads were then processed for paraffin embedding or OCT embedding for microtome or cryostat sectioning, respectively.

Microcomputed tomography (μCT)

After fixation, heads from three P19 K14$^{Cre/+}$;Adam10$^{fl/fl}$ and three wild-type mice were gradually dehydrated to 70% Ethanol and scanned at 70 kV and 114 μA with an isotropic resolution of 20 μm in a high-resolution μCT system (μCT 40, Scanco Medical). Three-dimensional (3D) reconstruction of the whole heads from the obtained slices was obtained using the software VGStudio MAX 2.0 (Volume Graphics GMBH).

Following the μCT evaluation, heads of P19 mice were divided in two-halves. One-half of each specimen was left fully mineralized and processed for examination in the scanning electron microscope (SEM). The other half was decalcified for 8 weeks in 10% ethylenediaminetetraacetic acid (EDTA) and then processed for paraffin embedding.

Scanning Electron Microscopy (SEM) evaluation and Toluidine Blue staining

SEM evaluation was processed as previously described (Luder and Amstad-Jossi, 2012). Briefly, heads were dehydrated in ethanol and embedded in Technovit 7200 VLC (Heraeus Kulzer, Wehrheim, Germany). Light-polymerized blocks were mounted on aluminum stubs, polished, and coated with a 10–15 nm thick layer of carbon. Thereafter, they were examined using a Tescan VEGA TS5316 XM SEM (Tescan, Brno, Czech Republic) operated in BSE mode. Micrographs were recorded at 20 kV¨ and a working distance of 23 mm. Immediately after SEM evaluation, the samples were sectioned (50 μm thick) (EXAKT 300 CL or CP) and stained with Toluidine Blue.

Transmission Electron Microscopy (TEM)

P19 mice were perfused with 4% PFA/0.2% glutaraldehyde in 0.1 m phosphate buffer pH 7.2. The mandibles were carefully dissected out and additionally fixed with 4% PFA overnight at 4°C, washed several times with PBS (PBS) and then decalcified with 10% EDTA for 8 weeks. Upon decalcification, the specimens were washed overnight in 0.185molL^{-1} Sodium cacodylate buffer (pH 7.4), post-fixed for 3 h at room temperature (RT) in 1.33% osmium tetroxide buffered in 0.067molL^{-1}s-Collidine (2,4,6 Trimethylpyridine), gradually dehydrated in ethanol, transferred to propylene oxide and finally embedded in Epon® 812 (Fluka AG, Buchs, Switzerland). From the resin blocks, 60–80 nm thin sections were cut using diamond knives (Diatome, Biel, Switzerland) in the Reichert OM-U2 ultramicrotome (Leica Microsystems, Heerbrugg, Switzerland). Sections were collected on copper-grids, contrasted with U-acetate and Pb-citrate, and examined in a Philips EM400 T TEM (FEI, Eindhoven, the Netherlands) at 60 kV. Micrographs were recorded using a Hamamatsu ORCA-HR camera (Hamamatsu Photonics, Hamamatsu, Japan) and the AMT image acquisition software (Deben, Bury St. Edmunds, UK).

Histological evaluation

Dehydrated wild-type and mutant tissue samples from different stages were paraffin embedded and sectioned to 5 μm thick sections. Hematoxylin and eosin (H&E) staining was used for the histological analysis of these samples.

Orientation analysis of ameloblasts

Orientations of the symmetry axis of ameloblasts nuclei in wild-type and K14$^{Cre/+}$;Adam10$^{fl/fl}$ incisors was measured by rotating a vector over the images and determining the angle between the basal and apical poles of the nuclei. Student's t-tests were used for statistical analyses.

In situ hybridization

Notch1, *Notch2* (Mitsiadis et al., 1995, 1998), *Adam10* (a gift from Prof. Yufang Zheng), *Ameloblastin* (*Ambn*; a gift from Dr Yoshihiko Yamada) riboprobes were used for *in situ* hybridization on 14 μm cryosections, as previously described (Mitsiadis et al., 1998). The hybridization signal was detected using the NBT/BCIP substrate solution, sections were mounted with Glicergel® mounting medium (Dako) and imaged with Leica DM6000 microscope equipped with the Leica DFC420C camera. Images were processed with the Leica Application Suite (LAS) software.

Immunostaining and immunofluorescence on sections and as whole mount

Polyclonal primary antibodies against amelogenin (Abcam, ab59705; 1:100), Adam10 (R&D Systems, mab946: 1:100), Keratin14 (Covance, PRB-155P-100; BioLegend, 905301; 1:100), Notch1 and Notch2 (Mitsiadis et al., 1995); 1:100) and Phospho-Histone3 (pH3; Santa Cruz, sc-8656-R; 1:100) were used.

5 μm paraffin sections and 14 μm cryosections were used for immunostaining and immunofluorescence, respectively. Deparaffinized sections were rehydrated, washed in PBS and permeabilized with 0.1% Triton X-100 before immunostaining. The sections were then incubated overnight at 4°C with primary antibodies diluted in 0.2% bovine serum albumin (BSA) in PBS, followed by PBS washes and incubation with the biotinylated secondary antibody for 1 h at RT. After washing in 0.2 BSA/PBS, the sections were finally incubated with Peroxidase-conjugated Streptavidin for 10 min. The signal was revealed with 3-Amino-9-Ethylcarbazole (AEC) reaction solution. In control sections the primary antibodies were omitted. For immunofluorescence, cryosections were dried for 1 h at RT, then washed with 0.2% BSA/PBS and incubated with primary antibodies overnight at 4°C. After several washes in 0.2% BSA/PBS the sections were incubated with either Alexa488 (Invitrogen, A21206) or Alexa568-conjugated (Invitrogen, A78946) secondary

antibodies for 45 min at RT. The sections were then shortly incubated with DAPI (4′,6-diamidino-2-phenylindole; Thermo Fisher Scientific) and mounted with DABCO (1,4-Diazabicyclo(2.2.2)Octan; Sigma-Aldrich) mounting medium and analyzed with either a Leica DM6000 FS or a Leica SP5 confocal microscope. Images were taken using the Leica DFC350FX camera and the Leica Application Suite Advanced Fluorescence (LAS AF) software.

For whole mount staining, incisors were fixed in 1% PFA in PBS for 1 h at RT, followed by permeabilization and blocking with 0.3% Triton X-100/10% Normal Horse Serum (NHS)/0.2% BSA in PBS overnight. Samples were incubated with primary antibodies for four days at 4°C, followed by 10 h wash with PBS. The incisors were then incubated with Alexa488 secondary antibody for 2 days at 4°C, followed by incubation with DAPI overnight at 4°C. Samples were then cleared with the clearing agent FocusClear© (CelExplorer, Taiwan, FC-101) and mounted with 2.5% 1,4-Diazobicyclo-[2.2.2]-Octane (DABCO; Sigma-Aldrich, D2522) for analysis under a Leica SP5 confocal microscope.

Terminal deoxynucleotidyl transferase-mediated dUTP nick end labeling (TUNEL)

TUNEL assay was performed on paraffin sections using terminal deoxynucleotidyl transferase (TdT) enzyme (Roche, 1176730500) and biotinylated dUTP (Roche, 11388908910). Briefly, samples were deparaffinized, rehydrated, and treated with a mixture of TdT enzyme and biotinylated dUTP. Sections were incubated briefly with DAPI and mounted with 2.5% DABCO. Pictures were taken using the Leica DFC350FX camera and the LAS AF software.

In vitro and *ex vivo* cultures of embryonic and postnatal incisors

Twelve E13.5 mouse incisors were dissected and cultured in semisolid medium consisted of 20% Fetal Bovine Serum (FBS; GIBCO®, Life Technologies), 1% Penicillin/Streptomycin (GIBCO®, Life Technologies), 1% L-Glutamine (GIBCO®, Life Technologies), 1.8 mg/mL Ascorbic Acid (Sigma-Aldrich) and 5% agarose (low EEO, Conda) in DMEM medium (GIBCO®, Life Technologies), with either 5 μM GI254023X (Sigma-Aldrich, SML0789) compound, which has been successfully used in previous *in vitro* and *in vivo* studies (Inoshima et al., 2012; Ludwig et al., 2005; Mizuno et al., 2018), or DMSO (control). Samples were harvested after 7 days in culture, fixed for 30 min in 4% PFA and processed for paraffin embedding. Six of the collected incisors (3 control and 3 treated with GI254023X) were then transplanted under the kidney capsule of immunocompromized *Rag1*−/− mice and cultured *ex vivo* for additional 7 days, as previously described (Jimenez-Rojo and Mitsiadis, 2019).

PN2 mouse incisors were isolated from Notch1$^{CreERT2/+}$;R26$^{mT/mG}$ pups and cultured in DMEM supplemented with 20% FBS, 1x Penicillin/Streptomycin, 1% L-Glutamine and 1.8mg/mL Ascorbic Acid, on an orbital shaker for 24 h. Incisors were then incubated with 100 nM 4-Hydroxytamoxifen (4-OHT; Sigma-Aldrich, H7904) for 2 h. Following tamoxifen removal, the samples were cultured for additional 4 days in the previously described medium. After the culture, samples were collected, washed several times with PBS, fixed in 1% PFA for 1 h and washed again with PBS. The samples were then cleared with the Focus Clear© (CelExplorer, Taiwan, FC-101) clearing agent for 3 days at 4°C and imaged with a Leica SP8 confocal laser scanning microscope. Images were analyzed with Fiji (Schindelin et al., 2012) and Imaris 9.0 (Bitplane, Belfast, Northern Ireland).

Alkaline Phosphatase (ALP) activity

ALP activity was assessed in paraffin sections. Briefly, sections were deparaffinized, rehydrated, and incubated in 1% $MgCl_2$ (Sigma-Aldrich, M8266) in Tris-Maleate buffer overnight at 4°C, followed by the addition of NBT/BCIP substrates (Sigma-Aldrich). Sections were finally mounted with Glicergel® mounting medium (Dako) and analyzed using a Leica DM6000 microscope.

QUANTIFICATION AND STATISTICAL ANALYSIS

Quantified proliferation data were analyzed by Student's *t* test using GraphPad Prism software, and p values <0.05 were considered statistically significant.